Cell

IGSF8 is an innate immune checkpoint and cancer immunotherapy target

Graphical abstract

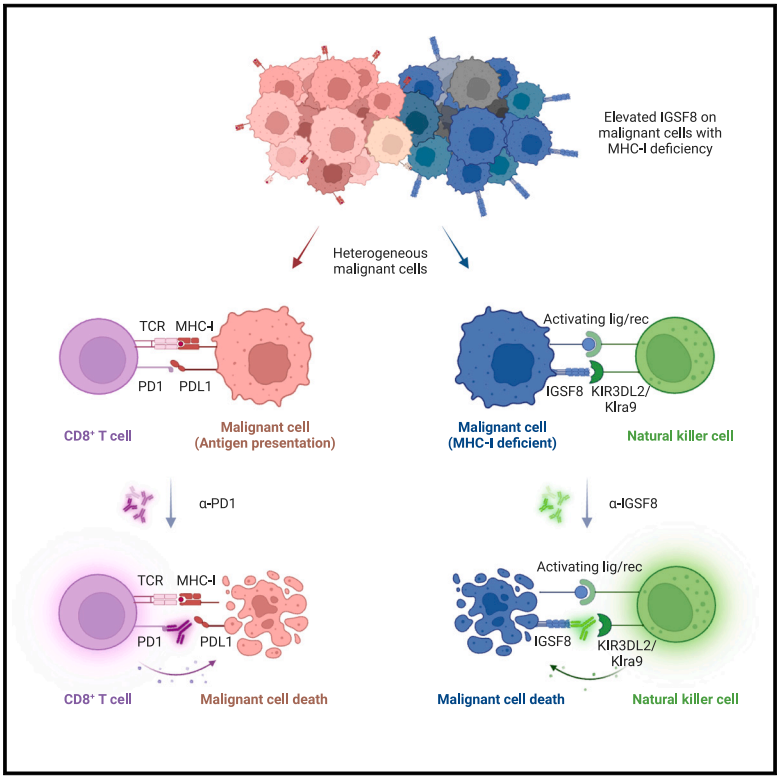

Authors

Yulong Li, Xiangyang Wu, Caibin Sheng, ..., Xihao Hu, X. Shirley Liu, Tengfei Xiao

Correspondence

xihao_hu@gv20tx.com (X.H.), xsliu@gv20tx.com (X.S.L.), tengfei_xiao@gv20tx.com (T.X.)

In brief

IGSF8, aberrantly expressed on malignant cells, functions as an innate immune checkpoint that inhibits cytotoxicity of natural killer cells. A monoclonal antibody targeting IGSF8 alone, or in combination with immune checkpoint blockade, shows therapeutic potential in preclinical models.

Highlights

- IGSF8 is highly expressed on malignant cells with antigen presentation defects
- IGSF8 interacts with NK receptors to suppress NK cell cytotoxicity
- Anti-IGSF8 antibody increases NK cell killing of malignant cells *in vitro*
- Anti-IGSF8 alone or in combination with anti-PD1 inhibits tumor growth *in vivo*

Li et al., 2024, Cell *187*, 1–14
May 23, 2024
https://doi.org/10.1016/j.cell.2024.03.039

Please cite this article in press as: Li et al., IGSF8 is an innate immune checkpoint and cancer immunotherapy target, Cell (2024), https://doi.org/10.1016/j.cell.2024.03.039

Cell

CellPress

Article

IGSF8 is an innate immune checkpoint and cancer immunotherapy target

Yulong Li,[1,3] Xiangyang Wu,[1,3] Caibin Sheng,[2,3] Hailing Liu,[1,3] Huizhu Liu,[1,3] Yixuan Tang,[1,3] Chao Liu,[1,3] Qingyang Ding,[1,3] Bin Xie,[1,3] Xi Xiao,[1,3] Rongbin Zheng,[1,3] Quan Yu,[1,3] Zengdan Guo,[1] Jian Ma,[1] Jin Wang,[1] Jinghong Gao,[1] Mei Tian,[1] Wei Wang,[1] Jia Zhou,[1] Li Jiang,[1] Mengmeng Gu,[1] Sailing Shi,[1] Michael Paull,[2] Guanhua Yang,[1] Wei Yang,[2] Steve Landau,[2] Xingfeng Bao,[2] Xihao Hu,[2,*] X. Shirley Liu,[2,*] and Tengfei Xiao[1,4,*]

[1]Shanghai Xunbaihui Biotechnology Co., Ltd., 3rd floor of Building 4, No. 3728, Jinke Road, Pudong New Area, Shanghai, 201203, China

[2]GV20 Therapeutics LLC, 237 Putnam Avenue, Cambridge, MA 02139, USA

[3]These authors contributed equally

[4]Lead contact

*Correspondence: xihao_hu@gv20tx.com (X.H.), xsliu@gv20tx.com (X.S.L.), tengfei_xiao@gv20tx.com (T.X.)

https://doi.org/10.1016/j.cell.2024.03.039

SUMMARY

Antigen presentation defects in tumors are prevalent mechanisms of adaptive immune evasion and resistance to cancer immunotherapy, whereas how tumors evade innate immunity is less clear. Using CRISPR screens, we discovered that IGSF8 expressed on tumors suppresses NK cell function by interacting with human KIR3DL2 and mouse Klra9 receptors on NK cells. IGSF8 is normally expressed in neuronal tissues and is not required for cell survival *in vitro* or *in vivo*. It is overexpressed and associated with low antigen presentation, low immune infiltration, and worse clinical outcomes in many tumors. An antibody that blocks IGSF8-NK receptor interaction enhances NK cell killing of malignant cells *in vitro* and upregulates antigen presentation, NK cell-mediated cytotoxicity, and T cell signaling *in vivo*. In syngeneic tumor models, anti-IGSF8 alone, or in combination with anti-PD1, inhibits tumor growth. Our results indicate that IGSF8 is an innate immune checkpoint that could be exploited as a therapeutic target.

INTRODUCTION

Immune checkpoint blockade (ICB) is a revolutionary approach to cancer treatment with exciting clinical efficacy. However, current ICB treatments benefit only a minority of cancer patients.[1] Two major mechanisms underlying this resistance to immunotherapy and immune evasion are T cell dysfunction and T cell exclusion.[2,3] Normally, $CD8^+$ T cells recognize neoantigens presented on malignant cells by major histocompatibility complex class I (MHC-I). T cells can kill malignant cells upon neoantigen recognition, but inhibitory molecules expressed on malignant cells often interact with T cells to induce T cell dysfunction. Current ICB antibodies can block this interaction and rejuvenate T cells that are at an early stage of dysfunction.[4,5] Besides T cell dysfunction, MHC-I loss has been reported in over 65% of all tumors and is a common mechanism of both primary and acquired resistance to ICB treatment.[6,7] MHC-I loss can occur through DNA mutations,[8] RNA down-regulation,[9] epigenetic silencing,[10] or protein degradation from autophagy.[11] These antigen-presentation-deficient tumors cannot be detected or destroyed by T cells and therefore often have low T cell infiltration (T cell exclusion) and are considered "immune cold" tumors. MHC-I normally acts as a marker of "self," and cells that lack MHC-I, for example due to viral infection,[12] are recognized and killed by Natural Killer (NK) cells. Considering the prevalence of tumors with MHC-I loss, we set out to solve a major puzzle in cancer immunology: why aren't tumors with MHC-I defects killed by NK cells?

RESULTS

A co-culture CRISPR screen identifies IGSF8 as an NK-cell checkpoint

We hypothesized that malignant cells with MHC-I defects express proteins to suppress NK cell function, thereby escaping NK cell activation and killing. To identify proteins with NK-cell checkpoint function, we conducted NK cell co-culture CRISPR screens in an MHC-I proficient COLO205 human colon cancer cell line and another MHC-I deficient[13] AGS human gastric cancer cell line. We infected the cells with lentiviral CRISPR knockout libraries (genome-wide library for COLO205 and cell surface gene library for AGS) and grew the infected cells for seven days *in vitro* (STAR Methods). The edited cells were then cultured alone or treated with expanded primary human NK cells (STAR Methods) overnight to identify genes whose knockout influences NK cell-mediated cancer cell killing (Figure 1A). CRISPR guide abundances from edited COLO205 or AGS cells with or without NK cell treatment were measured by high throughput sequencing, and differentially selected genes between the two

Please cite this article in press as: Li et al., IGSF8 is an innate immune checkpoint and cancer immunotherapy target, Cell (2024), https://doi.org/10.1016/j.cell.2024.03.039

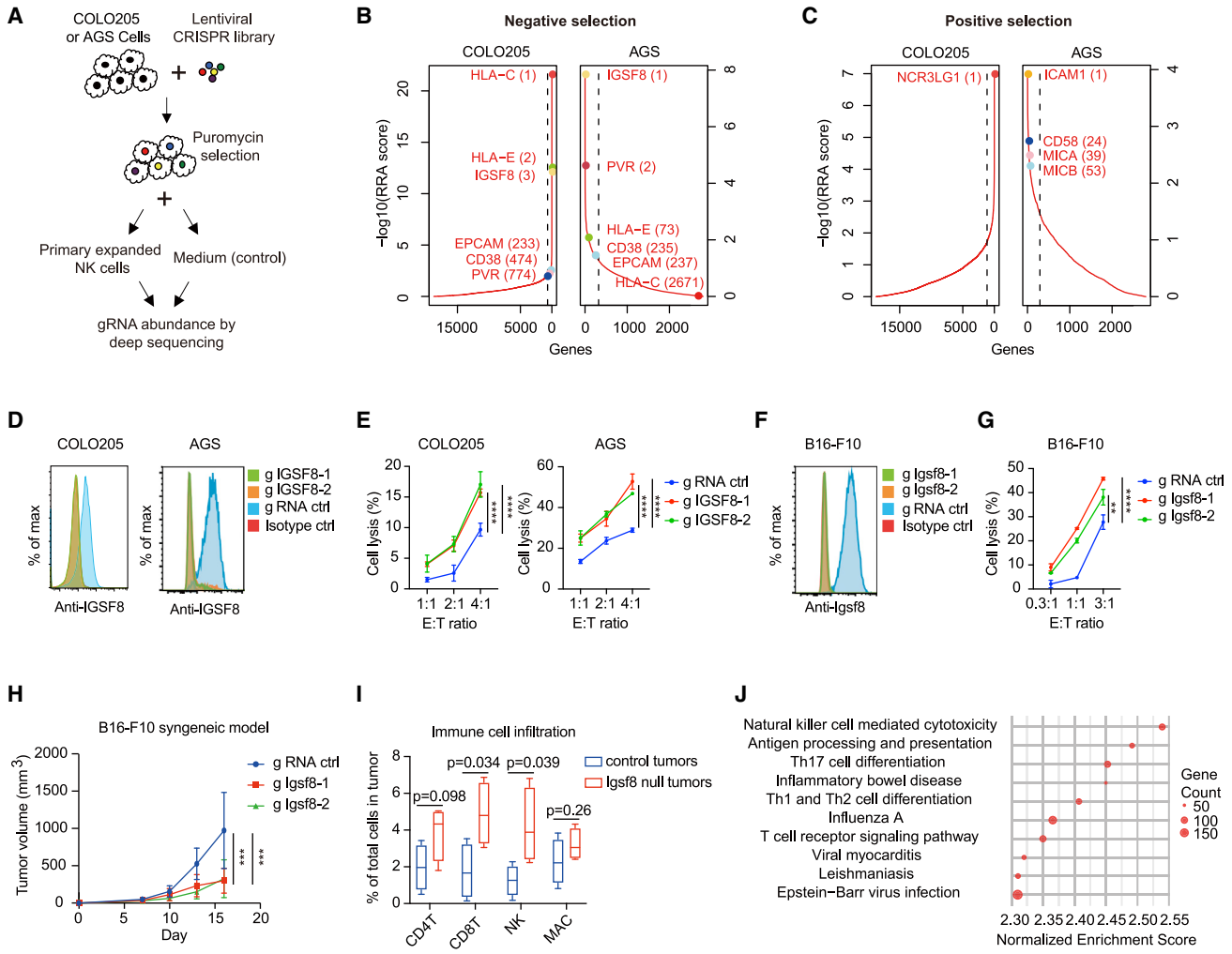

Figure 1. Identification of IGSF8 as a suppressor of NK cell killing

(A) Outline of the CRISPR screens in AGS or COLO205 and NK cell co-culture system.

(B and C) Negatively (B) or positively (C) selected genes in the AGS or COLO205 and NK cell co-culture screen. The top known genes under negative or positive selection were highlighted.

(D) Cell surface protein expression of IGSF8 on COLO205 (left) or AGS (right) control cells (human gAAVS1) and *IGSF8*-null cells (human gIGSF8-1/2) as measured by flow cytometry.

(E) Human NK cell-mediated cytotoxicity against COLO205 (left) or AGS (right) control and IGSF8-null cells by flow cytometric staining of COLO205 or AGS cells with viability dye (n = 3).

(F) Cell surface protein expression of Igsf8 on B16-F10 control cells (mouse gRosa26) and Igsf8-null cells (mouse gIgsf8-1/2) as measured by flow cytometry.

(G) Mouse NK cell-mediated cytotoxicity against B16-F10 control and Igsf8-null cells by flow cytometric staining of B16-F10 cells with viability dye (n = 3).

(H) Tumor growth of B16-F10 syngeneic model. Half a million of B16-F10 cells harboring either mouse gRosa26 (ctrl) or mouse gIgsf8 were inoculated subcutaneously into wild-type (WT) C57BL/6 mice (n = 8). Tumor volumes were measured at day 7, 10, 13, and 16.

(I) The infiltration of immune cells in both B16-F10 control and Igsf8-null tumors was analyzed using flow cytometry. The percentage (±SD) of each immune cell type among the total live cells in the tumors was plotted on the y axis (STAR Methods, n = 4, two-tailed Student's t test). MAC indicates $CD11b^+$ $F4/80^+$ macrophage.

(J) The most highly enriched Gene Set Enrichment Analysis (GSEA) pathways among upregulated genes in the B16-F10 Igsf8-null tumors compared to the control tumors. Data are represented as mean ± SD unless otherwise noted. Statistics: a two-way ANOVA test with Greenhouse-Geisser correction was used to calculate significance (E, G, and H). $^{**}p < 0.01$, $^{***}p < 0.001$, $^{****}p < 0.0001$. See also Figure S1.

treatment conditions were identified by the MAGeCK algorithm.[14]

We were interested in negatively selected genes whose knockout renders the malignant cells more sensitive to NK cell killing (negatively selected) and indeed found many genes well known to inhibit NK cell killing. For example, MHC-I members, including HLA-C that binds to KIR2D family receptors,[15] and HLA-E that binds to NKG2A[16] were the strongest hits in COLO205 (Figure 1B; Table S1) but were much weaker in the MHC-I defective AGS cells (Figure 1B; Table S2). Other

negatively selected genes common between the two cell lines, such as EPCAM,[17] CD38,[18] and PVR,[19,20] were previously reported NK-cell suppressors. The top positively selected genes, although slightly different in the two cell lines, were also well-known activating ligands for NK cells, such as NCR3LG1[21] in COLO205; ICAM1;[22] MICA/B;[23] and CD58[24] in AGS (Figure 1C). Strong negative and positive selection of genes expected to be involved in NK cell killing based on known mechanisms support the methodology used and the validity of the NK cell co-culture CRISPR screens results.

In addition to the expected targets, IGSF8 consistently appeared as a strong negatively selected gene in both screens (Figure 1B). It also showed moderate negative selection in previously published CRISPR screens in the K562 leukemia cell line co-cultured with NK cells[25] (Figure S1A). IGSF8 (also known as EWI-2, CD316, LIR-D1) is a member of the EWI subfamily of the immunoglobulin superfamily and has been reported to associate with the tetraspanins CD81 and CD9 on the same cells,[26] potentially regulating cell migration[27] and viral infection.[28,29] IGSF8 was also reported to have tumor suppressor-like properties in glioma and glioblastoma,[30] although few published studies directly interrogated IGSF8 function. CRISPR screens on hundreds of cancer cell lines grown under baseline conditions (in the absence of immune cells) from the DepMap project[31] suggest that IGSF8 has no major effects on cancer cell survival (Figures S1B and S1C).

To test the hypothesis that loss of IGSF8 in malignant cells enhances NK-cell killing, we used two different CRISPR gRNAs to knockout IGSF8 in COLO205 and AGS cancer cell lines and observed significantly increased killing by primary NK cells (Figures 1D and 1E). In H520 non-small cell lung cancer and K562 leukemia cell lines, loss of IGSF8 also promoted NK cell killing (Figures S1D and S1E), suggesting a general inhibitory function of IGSF8 in different cancer types. We examined whether IGSF8 might suppress NK cell function through regulating MHC-I levels in malignant cells. However, IGSF8 knockout resulted in little change in human leukocyte antigen (HLA) or MHC-I member B2M expression at either the RNA (Figure S1F) or protein (Figure S1G) level in COLO205 and AGS cells. Conversely, B2M knockout did not alter either the IGSF8 mRNA (Figure S1H) or protein expression (Figure S1I). In addition, IGSF8 was not a hit in previously published CRISPR screens[32] aiming to identify regulators of cell-surface MHC-I expression, indicating that IGSF8 suppression of NK cytotoxicity could be mediated by an MHC-I-independent mechanism. We next hypothesized that IGSF8 might suppress NK cytotoxicity by reducing NK cell degranulation. Indeed, IGSF8 overexpression in K562 cells significantly inhibited the expression of degranulation marker CD107a[33] on NK cells derived or expanded from human peripheral blood mononuclear cells (PBMC) during co-culture, an effect comparable to HLA-C overexpression (Figure S1J). Moreover, overexpression of IGSF8 suppressed NK-cell killing of K562 cells (Figure S1K). These observations indicate that IGSF8 inhibits NK cell-mediated cytotoxicity by suppressing degranulation.

IGSF8 is an evolutionarily conserved gene, having 90% sequence identity between human and mouse. The mouse *Igsf8* gene also showed negative selection in two published NK cell-co-culture CRISPR screens, one using the mouse MC38 colorectal cancer cell line,[34] and the other using the mouse MHC-I defective[35] B16-F10 melanoma cell line[36] (Figures S1L and S1M). To validate this phenotype, we used two different CRISPR gRNAs to knock out *Igsf8* in B16-F10 and observed significantly increased NK cell killing (Figures 1F and 1G), suggesting that IGSF8 suppression of NK cells is conserved between human and mouse. In addition, while *Igsf8* knockout has little effect on B16-F10 cell growth *in vitro* (Figure S1N), it dramatically reduced tumor growth in the C57BL/6 syngeneic mice *in vivo* (Figure 1H). Flow cytometry of the tumor-infiltrating $CD45^+$ cells revealed that *Igsf8* knockout in B16-F10 resulted in significantly increased NK and CD8 T cells and little effect on macrophages (Figure 1I). Comparing RNA-seq profiles of B16-F10 tumors with or without *Igsf8* knockout collected 17 days after implantation revealed that *Igsf8* knockout in tumors resulted in remarkable up-regulation of NK cell-mediated cytotoxicity, increases in antigen processing and presentation, and T cell signaling (Figures 1J and S1O; Table S3). Together, our results suggest that IGSF8 is an NK-cell checkpoint and novel immunotherapy target.

IGSF8 interacts with specific NK receptors to suppress NK cell function

IGSF8 protein normally has a weak interaction with resting NK cells in PBMC, but this interaction was markedly enhanced in the expanded NK cells that were used in our CRISPR screens (Figures 2A and 2B; STAR Methods). To identify the IGSF8 binding partner on human NK cells, we took two different approaches. First, we sorted expanded NK cells below the 10^{th} and above the 90^{th} percentile of binding to IGSF8 protein to find genes that might be responsible for the differential binding (Figure S2A). Comparing the RNA-seq profiles between the two cell populations, we found KIR3DL2 to be the top cell surface receptor with differential expression (Figure 2C; Table S4). Second, we conducted CRISPR screens by transfecting primary expanded NK cells with a lentiviral gRNA pool targeting all cell surface proteins and introducing the Cas9 protein by electroporation (Figure S2B; STAR Methods). We cultured the NK cells for seven days *in vitro* to complete gene knockout, then sorted the NK cells below the 10^{th} and above the 90^{th} percentile of binding to IGSF8 protein. By comparing CRISPR gDNA abundance between the two cell populations, we again identified *KIR3DL2* as a gene whose loss in NK cells decreases IGSF8 binding to NK cells (Figure S2C; Table S5).

KIR3DL2 is a member of the killer cell immunoglobulin-like receptors (KIRs), a family of proteins known to interact with MHC-I to inhibit NK cell function.[37] 3D structural modeling revealed that IGSF8 exhibits high structural similarity (TM-score > 0.5) with the alpha3 domain of human and mouse MHC-I and B2M proteins (Table 1), supporting IGSF8 binding to KIR3DL2 in place of MHC-I/B2M. We validated the specific interaction between KIR3DL2 and IGSF8 with several approaches. First, using surface plasmon resonance, we measured the affinity of KIR3DL2-IGSF8 interaction to be 0.654 μM (Figure S2D). Second, we expressed the Fc-fusion protein of six different KIR family members and found that only KIR3DL2 can bind to mouse CT26 cells overexpressing IGSF8 (Figure 2D). We also overexpressed different KIR family genes on CT26 cells and found only CT26-KIR3DL2 cells to bind to IGSF8 protein (Figure S2E). The interaction

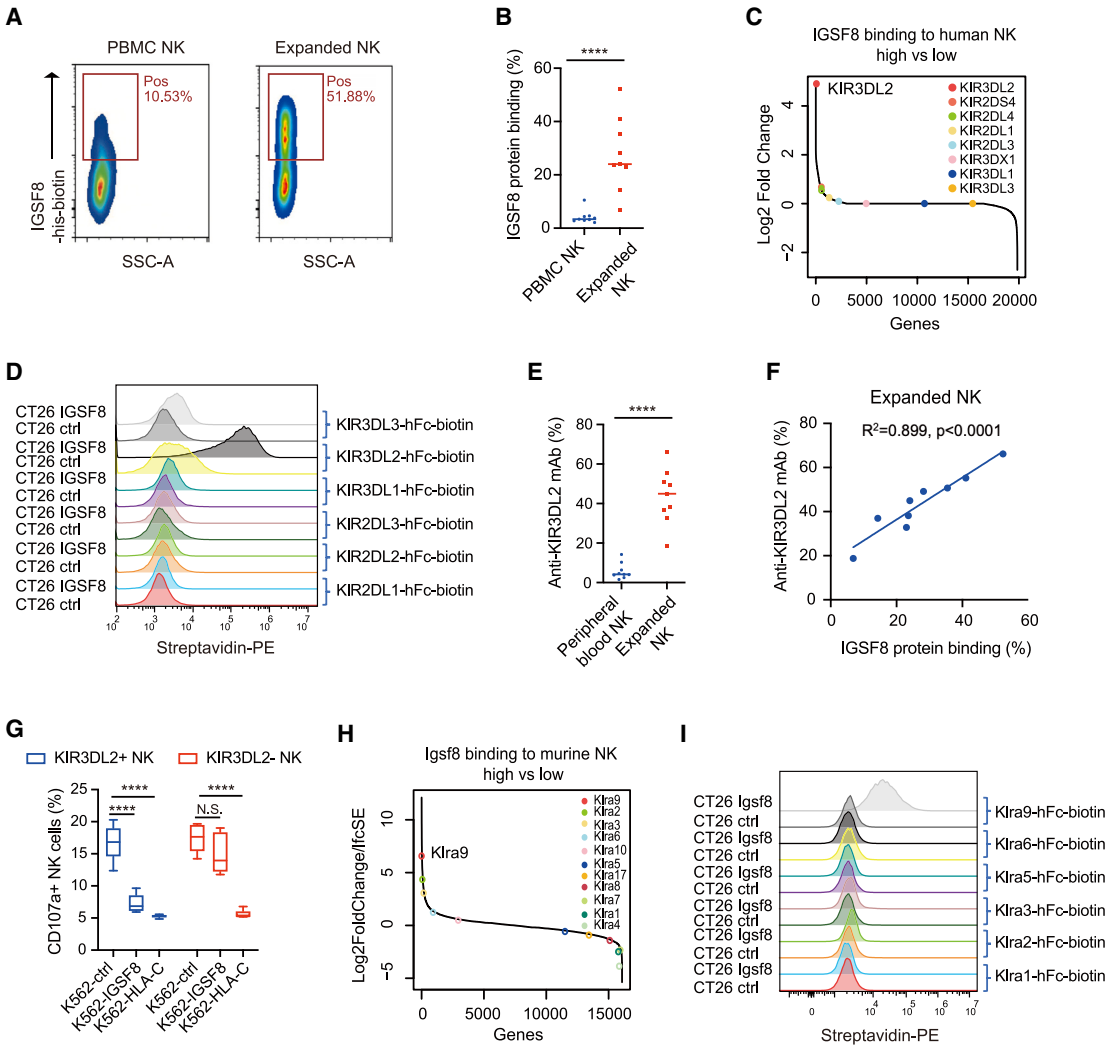

Figure 2. Identification of KIR3DL2 and Klra9 as the binding partner of IGSF8 on NK cells

(A and B) Representative figures (A) and summary (B). The data display the percentage of CD56$^+$ NK cells expressing the putative IGSF8 binding partner in peripheral blood samples collected from nine healthy donors. The samples were collected both before (blue, left) and after (red, right) *ex vivo* expansion of human NK cells. Expression of the putative IGSF8-binding partner was detected by biotinylated human IGSF8-his recombinant protein (n = 9).

(C) Rank plot of mRNA expression based on the log 2-fold difference in mRNA expression, comparing the top 10% and bottom 10% of expanded NK cells based on their binding to the IGSF8 protein. The top hit, KIR3DL2, and other genes in the KIR family are highlighted.

(D) Flow cytometry staining of CT26 cells transduced with either human IGSF8 cDNA or with an HA tag (control). KIR extracellular domains were produced with a human Fc tag in CHO cells and biotinylated. Overlay histograms show the binding of the KIR proteins to CT26 cells overexpressing IGSF8 or to control cells.

(E) Flow cytometry on CD56$^+$ NK cells using an anti-KIR3DL2 monoclonal antibody. Each dot shows the percentage of NK cells that express KIR3DL2 on the cell surface collected from a healthy donor before (blue) and after (red) *ex vivo* expansion (n = 9).

(F) Simple linear regression between the percentage of expanded NK cells expressing KIR3DL2 (y axis) and the percentage of NK cells that bound biotinylated IGSF8-his protein (x axis).

(G) NK cell-mediated cytotoxicity. NK cells were co-cultured with K562 overexpressing IGSF8 or HLA-C or HA-tag control for 4 h. Boxplots show mean ± SD (n = 5).

(H) A rank plot of mRNA expression based on the log 2-fold/lfcSE difference in mRNA expression, comparing the top 10% and bottom 10% of NK-cell binding to mouse Igsf8 protein (n = 3). Klra9, and other Ly49 family genes are highlighted.

(I) Flow cytometry staining of CT26 cells transduced with either mouse Igsf8 cDNA or HA tag (control). The extracellular domains of Klra1, 2, 3, 5, 6, and 9 were produced with a human Fc tag in CHO cells and biotinylated. Overlay histograms show the binding of Klra proteins to CT26 cells overexpressing Igsf8 or to control cells. Statistics: two-tailed Student's t test (B, E, and G). ****$p < 0.0001$. See also Figure S2.

between IGSF8 protein and CT26-KIR3DL2 cells could be fully blocked by a commercially available KIR3DL2-specific antibody (MAB2878) (Figure S2F). Third, IGSF8 protein binds to engineered NK92 cells expressing KIR3DL2, but not to wild-type NK92 cells that do not express KIR3DL2 (Figures S2G and S2H). Fourth, KIR3DL2 expression was significantly increased

Table 1. Comparative analysis of the protein tertiary structures between IGSF8 and human or mouse MHC class I-B2M complexes

	IGSF8_ECD	IGSF8_D1	IGSF8_D2	IGSF8_D3	IGSF8_D4
H-2Kb_alpha1	0.4031	0.4031	0.4174	0.3904	0.3721
H-2Kb_alpha2	0.372	0.3974	0.4057	0.3887	0.3427
H-2Kb_alpha3	0.5528	0.5528	0.5527	0.579	0.5867
mouse_B2M	0.6214	0.5417	0.5963	0.6049	0.6351
HLA-B*5701_alpha1	0.4206	0.3951	0.4267	0.4146	0.3499
HLA-B*5701_alpha2	0.3827	0.3966	0.4018	0.3637	0.3527
HLA-B*5701_alpha3	0.5614	0.5614	0.5375	0.5833	0.5882
human_B2M	0.6222	0.5397	0.5303	0.6056	0.6293

Note: TM-scores are normalized by the length of MHC-I/β2M domains.

on expanded NK cells (Figure 2E), consistent with the increased IGSF8 protein binding to these cells (Figure 2B). When testing expanded NK cells from nine different donors, we observed a significant positive correlation between KIR3DL2 expression on the expanded NK cells and IGSF8 binding to these cells (Figure 2F). Additionally, we observed comparable binding of IGSF8 protein or anti-KIR3DL2 antibody (MAB3878) to PBMC-derived NK cells that were co-cultured with K562 cells (Figure S2I). Furthermore, the binding of IGSF8 to expanded NK cells could be completely blocked by MAB2878 (Figure S2J). Finally, a recent high-throughput interaction screening study[38] of human immune cell surface receptors also identified IGSF8 and KIR3DL2 as each other's mutual top interaction partners (Figure S2K). Together, these results demonstrate a specific interaction between IGSF8 and the KIR3DL2 receptor on human NK cells.

We next sought to evaluate the effect of IGSF8-KIR3DL2 interaction on NK cell-mediated cytotoxicity with two experiments. First, we performed a co-culture experiment by incubating expanded primary NK cells with K562 cells overexpressing IGSF8, HLA-C, or HA-tag control, followed by flow cytometry analysis of the NK cells using antibodies against the degranulation marker CD107a or KIR3DL2. While K562-HLA-C inhibited degranulation in NK cells regardless of KIR3DL2 levels, K562-IGSF8 inhibited degranulation specifically in the KIR3DL2+ NK cells (Figure 2G). Second, we evaluated the cytotoxicity of NK92 and NK92-KIR3DL2 cells against K562 cells overexpressing IGSF8, HLA-C, or HA-tag control. Whereas NK92 cells, which express LILRB1 (Figure S2L), exhibited reduced killing of K562-HLA-C cells regardless of KIR3DL2 expression, NK92-KIR3DL2 cells showed reduced killing specifically against K562-IGSF8 cells (Figure S2M). These findings provide evidence that IGSF8 inhibits NK cell-mediated cytotoxicity through its specific interaction with KIR3DL2.

A challenge in identifying the IGSF8 binding partner in mice is that the expression of KIR3DL2 or other KIR family proteins is absent in mouse NK cells. Instead, the mouse genome possesses a counterpart receptor gene family Ly49 that closely resembles the human KIR family in both functional and genetic characteristics but is not expressed in humans.[39] To identify the Igsf8 mouse binding partner, we first collected mouse splenocytes and observed that NK cells exhibit stronger binding to mouse Igsf8 protein compared to T cells (Figure S2N). Comparing mRNA of pre-activated NK cells below the 10th and above the 90th percentile of binding to the mouse Igsf8 protein (Figure S2O), we found that the mRNA of Klra9 in the Ly49 family was significantly more abundant in NK cells that bind to the mouse Igsf8 protein (Figure 2H; Table S6). We then expressed different members of the Ly49 receptor family as human Fc (hFc) recombinant proteins and found that only Klra9 protein binds specifically to CT26-Igsf8 cells (Figure 2I). In humans, *KIR3DL2* is a framework gene in the KIR family, meaning that with few exceptions it is present in every individual, and is a known MHC-I receptor in humans.[40] Similarly, in mice, *Klra9* is a framework gene in the Ly49 family that interacts with MHC-I to inhibit NK cell function.[41] The mirrored functional and genetic characteristics of KIR3DL2 and Klra9 suggest that their interaction with IGSF8 plays a conserved function in regulating NK cells.

IGSF8 is highly expressed and associated with poor clinical outcomes in many cancers, and IGSF8 interaction with KIR3DL2 is independent of KIR3DL2 and HLA alleles

Normally, IGSF8 is most highly expressed in the brain and components of the central nervous system (CNS), while KIR3DL2 is expressed in spleen and whole blood, especially in NK cells (Figures S3A–S3C). Because neurons express little to no MHC-I,[42–45] the role of IGSF8 may contribute to the immune privilege of the CNS through NK cell suppression. In The Cancer Genome Atlas (TCGA) tumor profiles, IGSF8 mRNA is most abundant in melanoma and is significantly overexpressed in many solid tumor types (Figure 3A). IGSF8 also shows frequent copy number amplifications (Figure S3D), which is positively correlated with IGSF8 mRNA expression (Figure S3E), suggesting that it is expressed in malignant cells. Indeed, analysis of tumor single-cell RNA-seq data across 96 studies[46] confirmed that IGSF8 is most highly expressed in malignant cells (Figure 3B; STAR Methods). In contrast, KIR3DL2 has low overall expression and sparse copy number aberrations in TCGA cancer samples (Figures S3F and S3G) but is expressed uniquely in NK cells and T cells (Figure 3B).

In tumors profiled in the TCGA database, IGSF8 mRNA expression is negatively associated with CD8, granzyme, perforin, CD274 (PDL1), and MHC-I member B2M (Figure 3C). In addition, IGSF8 mRNA expression is significantly correlated with autophagy regulators that degrade MHC-I.[11,49–51] Furthermore, we observed frequent down-regulation of B2M and

Please cite this article in press as: Li et al., IGSF8 is an innate immune checkpoint and cancer immunotherapy target, Cell (2024), https://doi.org/10.1016/j.cell.2024.03.039

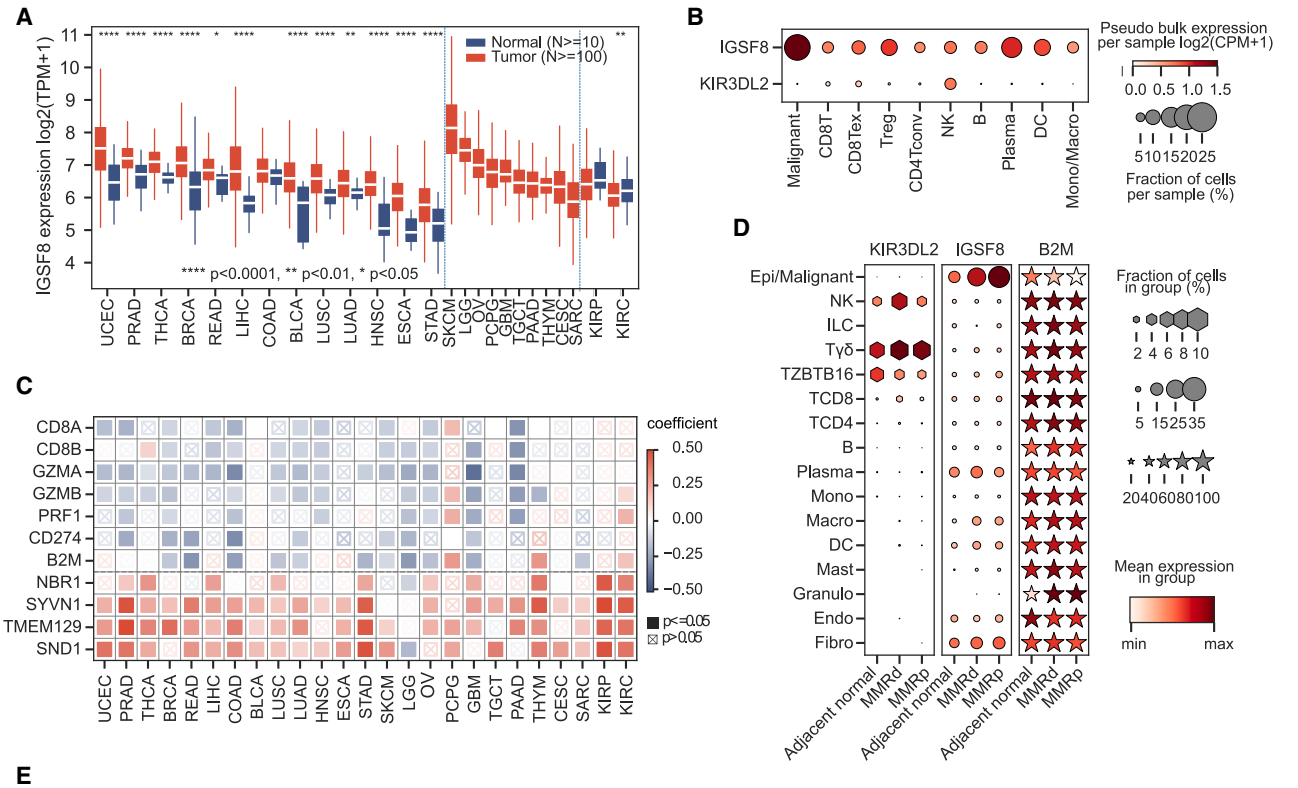

(legend on next page)

Please cite this article in press as: Li et al., IGSF8 is an innate immune checkpoint and cancer immunotherapy target, Cell (2024), https://doi.org/10.1016/j.cell.2024.03.039

up-regulation of IGSF8 mRNA expression in many cancer types in the TCGA database, especially non-small cell lung cancers and colorectal cancers (Figures S3H and S3I). These findings align with the scRNA-seq data obtained from colorectal tumors and adjacent normal tissues of 28 mismatch repair-proficient (MMRp) and 34 mismatch repair-deficient (MMRd) patients.[47] Within the authors' carefully curated cell annotations on this dataset, malignant cells exhibit a significant decrease in B2M expression and an increase in IGSF8 expression compared to adjacent normal epithelial cells, particularly in MMRp tumors (Figures 3D and S3J). Interestingly, KIR3DL2 is expressed on NK cells, but even higher in the non-MHC-I restricted γδ T cells, especially in the tumor tissues (Figure 3D). This observation, together with another study[52] showing that 90% of tumor-infiltrating PD1+ γδ T cells in MHC-I defective colorectal tumors have cell surface KIR3DL2 expression, suggests the potential involvement of KIR3DL2 and γδ T cells in antigen presentation-defective tumors. Together, our investigation in public data indicates IGSF8 is higher in tumors with poor immune infiltration, low susceptibility to cytotoxicity, antigen presentation defects, and resistance to anti-PD1 treatment. Interestingly, kidney cancers have distinct tumor immune microenvironment and ICB response profiles than other solid tumors,[53] and IGSF8 also behaves differently in kidney cancers than in other solid tumors, supporting its potential role as an immune checkpoint.

To evaluate whether IGSF8 and MHC-I are inversely expressed at the protein level, we first examined available proteomics data from Cancer Cell Line Encyclopedia (CCLE)[31] and Clinical Proteomic Tumor Analysis Consortium (CPTAC).[54,55] In general, IGSF8 mRNA and protein levels are significantly correlated in CCLE cell lines (Figure S3K) and tumors in the CPTAC database (Figure S3L). However, B2M and IGSF8 proteins have no correlation in CCLE cell lines (Figure S3M), consistent with our earlier observations that B2M and IGSF8 do not directly regulate each other *in vitro* (Figures S1G and S1I). B2M and IGSF8 also show no correlation in tumors in the CPTAC database (Figure S3N), potentially due to confounding MHC-I protein expression on stromal and immune cells in the tumors. Therefore, we conducted immunohistochemistry staining of lung cancer, colorectal cancer, breast cancer, and melanoma tumor slides (Figure S4A). Indeed, MHC-I was primarily located in stromal cells and often much lower or absent in malignant cells. In contrast, IGSF8 protein expression was primarily located in malignant cells, as evidenced by its co-localization with cytokeratin and confirmed by Hematoxylin and Eosin (H&E) staining (Figure S4A). Moreover, we observed a heterogeneous and inverse expression of MHC-I and IGSF8 proteins among different malignant cells within the same tumor samples (Figure 3E). This result suggests a potential role for IGSF8 in evading NK cell attack in tumors with MHC-I deficiency.

We further evaluated the relationship between IGSF8 mRNA expression and clinical outcomes. In cervical, endometrial, colon, non-small cell lung cancers, and melanoma in the TCGA database, among tumors with lower MHC-I expression, high IGSF8 expression is significantly associated with worse survival (Figures 3F and S4B). In one melanoma study with tumor profiles done before Pembrolizumab treatment,[56] whereas neither PD1 nor PDL1 expression distinguishes responders from non-responders, complete responders had significantly lower IGSF8 levels and significantly higher B2M levels (Figure S4C). In another melanoma study with tumor profiles before and during Nivolumab treatment,[48] IGSF8 level is significantly lower in the on-treatment tumors that benefited from Nivolumab (Figure 3G). These results suggest that good antigen presentation and low IGSF8 expression might be informative predictors or indicators of anti-PD1 response.

KIR3DL2 is highly polymorphic, with 62 reported protein coding allelic variants.[40] We experimentally tested nine of the most common KIR3DL2 variants annotated in a North American cohort[57] and found all of them bind strongly to IGSF8 (Figure 3H) and the KIR3DL2 antibody Lacutamab (Figure S4D). We also computationally annotated the top 11 most prevalent KIR3DL2 variants in tumors in the TCGA database,[58] which include the top nine variants in the North American cohort and cover 88.5% of the patient samples in the TCGA database. Although some of the KIR3DL2 variants are associated with differential KIR3DL2 expression (Figure S4E), none of them are associated

Figure 3. Evaluation of IGSF8 and KIR3DL2 gene expression profiles in patient tumors

(A) Differential expression of *IGSF8* in tumor (red) versus tumor-adjacent normal tissues (blue) in TCGA. Tumor types are categorized into three groups: "overexpression," "unknown," and "downregulation," and sorted by the IGSF8 expression levels in tumors. Differences assessed by two-tailed Student's t-test: $^{*}p < 0.05$, $^{**}p < 0.01$, $^{****}p < 0.0001$.

(B) Single-cell expression of IGSF8 and KIR3DL2 in malignant cells and immune cells. Data from approximately four million cells from 836 non-treated cancer patients were obtained from TISCH2. Pseudo-bulk expression and cell fraction are visualized using gradient color and dot size, respectively.

(C) Spearman's rank correlation between IGSF8 expression and selected genes. Across most TCGA tumor types, IGSF8 expression negatively correlates with CD8A, CD8B, GZMA, GZMB, PRF1, and B2M, while positively correlating with autophagy-related genes, including NBR1, SYVN1, TMEM129, and SND1. The correlation coefficient and statistical significance ($p \leq 0.05$) are represented by color and solid boxes, respectively.

(D) Cell-type-specific expression of IGSF8, KIR3DL2, and B2M in colorectal tumor and adjacent normal tissues from Pelka et al.[47] Normalized expression levels and the fraction of cells expressing the genes are represented by color and shape size (STAR Methods), respectively.

(E) Representative images of immunohistochemical staining with anti-IGSF8 (red), anti-HLA-A/B (blue) and H&E on tissue sections of lung tumors. The "merge" image illustrates inverse expression of IGSF8 and MHC-I within the same tumor sections. White box indicates the zoomed area shown below each tissue section.

(F) Hazard ratios associated with IGSF8 expression in patients with relatively low antigen presentation (MHC low, STAR Methods) in six TCGA cancer types. Cox multivariate regression was conducted to determine the hazard ratio for IGSF8, with corresponding *p* values presented.

(G) Comparison of IGSF8 expression in patients, stratified by response to anti-PD1 treatment (blue: pre-treatment, red: on-treatment). RNA-seq data from GEO accession number GSE91061.[48] "Benefit" group: complete response, partial response, and stable disease; "Non-benefit" group: progressive disease. Statistical analysis were performed using two-tailed Student's t-test and Wilcoxon rank-sum test (U-test).

(H) Flow cytometric staining of CT26 cells with exogenous expression of nine KIR3DL2 variants or the HA tag (control) by lentiviral vector. Overlay histograms show the binding of IGSF8 proteins to CT26 cells with different KIR3DL2 variants or control tag. See also Figures S3 and S4.

Please cite this article in press as: Li et al., IGSF8 is an innate immune checkpoint and cancer immunotherapy target, Cell (2024), https://doi.org/10.1016/j.cell.2024.03.039

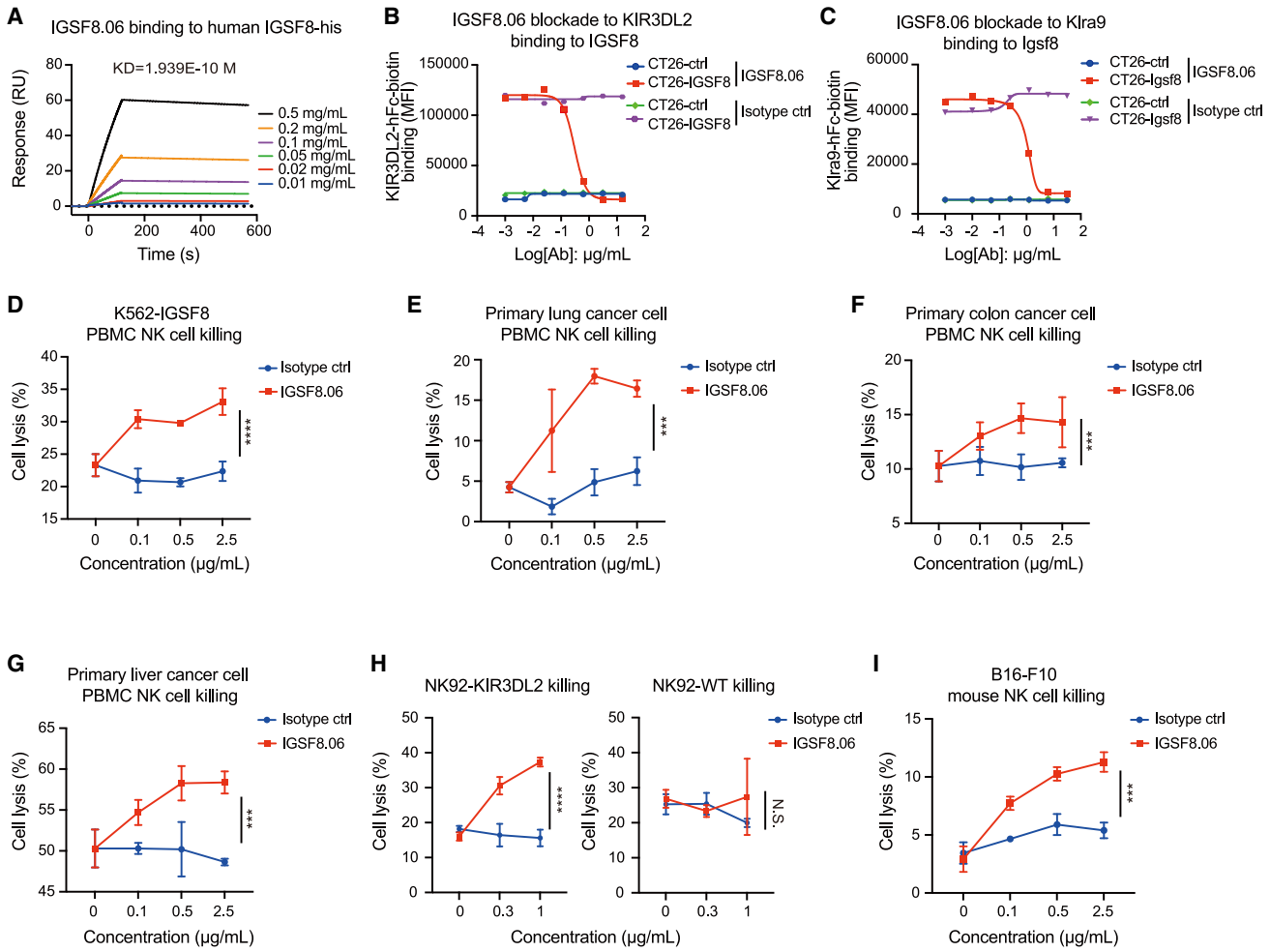

Figure 4. Development of an anti-IGSF8 antibody to activate NK cell-mediated cytotoxicity

(A) Surface plasmon resonance (SPR) sensorgrams of the anti-IGSF8 antibody (IGSF8.06).

(B) The effect of IGSF8.06 or isotype-matched control antibody on the binding of biotinylated KIR3DL2 recombinant protein to CT26 cells transduced with human IGSF8 or HA tag (control). MFI, mean fluorescence intensity.

(C) same as (B), using Klra9-hFc recombinant protein and mouse Igsf8.

(D) Dose-response curve on the effect of varying concentrations (x axis) of IGSF8.06 (red) or isotype-matched control IgG (blue) (both with IgG1-LALA Fc) treatment on K562-IGSF8 cell lysis (y axis). Human primary PBMC NK cells from a healthy donor were co-cultured with K562 cells overexpressing IGSF8 at a 1:1 E:T ratio with antibody treatment for 4 h.

(E–G) Same as (D), but with primary lung (E), colon (F), and liver (G) malignant cells.

(H) Engineered NK92-KIR3DL2 or wild-type NK92 cells were co-cultured with COLO205 cells at a 2:1 E:T ratio with varying concentrations of IGSF8.06-IgG1-LALA (red) or IgG1-LALA isotype-matched control (blue) antibody overnight.

(I) Same as (D), but with mouse primary NK cells evaluated against B16-F10 cells at a 1:1 E:T ratio overnight. Data are represented as mean ± SD ($n = 3$). Statistics: a two-way ANOVA test was used to calculate significance (D–I). ***$p < 0.001$, ****$p < 0.0001$. See also Figure S5.

with differential IGSF8 expression in tumors in the TCGA database (Figure S4F). We further examined the known KIR3DL2 ligands HLA-A3 and A11[59] but failed to identify a significant association between HLA-A3/A11 and KIR3DL2 mRNA expression (Figure S4G), IGSF8 mRNA (Figure S4H), or protein expressions (Figure S4I) in tumors in the TCGA database. In addition, the presence of HLA-A3 or A11 alleles in patients in the TCGA database does not seem to impact the association of IGSF8 with survival outcomes (Figure S4J). Together these data suggest that IGSF8-KIR3DL2 interaction might be independent of KIR3DL2 or HLA allele variants.

An antibody that blocks IGSF8 interaction with its NK receptors enhances NK cell killing

The Mouse Genome Database[60] reports only minor metabolic and diabetic phenotypes for *Igsf8*-null mice, so we reasoned that systemically blocking IGSF8 by an antibody may be well tolerated. We developed an antibody (IGSF8.06) against IGSF8 to block the interaction between IGSF8 and its binding partners. The antibody binds with high affinity (KD = 0.19 nM) to human IGSF8 (Figure 4A) and cross-reacts with mouse Igsf8 (Figure S5A). IGSF8.06 also has high specificity since it doesn't bind to *IGSF8*-null malignant cells even at a high antibody concentration (100 μg/mL) (Figure S5B).

Biolayer Interferometry experiments demonstrated that the IGSF8.06 antibody specifically blocks the interaction between KIR3DL2 and IGSF8 proteins (Figure S5C). In addition, flow cytometry experiments confirmed that IGSF8.06 antibody specifically blocks KIR3DL2 binding to CT26 cells overexpressing human IGSF8 (Figure 4B) or Klra9 binding to CT26 cells overexpressing mouse Igsf8 (Figure 4C). The IGSF8.06 antibody contains an L234A/L235A (LALA) mutation in the Fc region to eliminate potential Fc-dependent effector functions.

We first assessed the Fc-silent IGSF8.06 antibody function *in vitro* and found it to significantly enhance the cytotoxicity of expanded NK cells against AGS and COLO205 cells (Figures S5D and S5E). The antibody also increased the killing of PBMC-derived NK cells against K562 cells overexpressing either IGSF8 (Figure 4D) or HLA-C (Figure S5F). Next, we tested commercially obtained, cultured primary lung, colon, and liver malignant cells with detectable IGSF8 and MHC-I expression (Figure S5G) and again observed elevated PBMC-derived NK cell killing of these malignant cells upon IGSF8.06 treatment (Figures 4E–4G). To investigate whether the activation of NK cells by IGSF8.06 antibody depends on KIR3DL2, we tested IGSF8.06 antibody on COLO205 or K562-IGSF8 malignant cells co-cultured with NK92 or NK92-KIR3DL2 cells. While IGSF8.06 antibody significantly increased the killing of COLO205 or K562-IGSF8 cells by NK92-KIR3DL2 cells, it did not affect the killing of COLO205 or K562-IGSF8 cells by wild-type NK92 cells (Figures 4H and S5H). Furthermore, IGSF8.06 antibody significantly boosted the cytotoxicity of expanded mouse spleen-derived NK cells with Klra9 expression (Figure S5I) against the mouse melanoma B16-F10 cells (Figure 4I). Together, these results demonstrate that the IGSF8.06 antibody enhances NK cell killing of malignant cells by blocking IGSF8 interaction with its NK receptors.

The anti-IGSF8 antibody has remarkable anti-tumor effects *in vivo*

We tested the *in vivo* efficacy of the Fc-silent IGSF8.06 antibody in the B16-F10 syngeneic tumor model. We observed remarkable *in vivo* efficacy as measured by tumor growth inhibition (Figure 5A) and mouse survival (Figure S6A). In three out of eight mice, the B16-F10 tumors completely disappeared, and these mice remained tumor-free beyond the end of the experiment (58 days), whereas all mice in the control group had to be sacrificed by day 25 due to large tumor size (Figure S6A). Flow cytometry of the tumor-infiltrating $CD45^+$ cells from the harvested tumors revealed that IGSF8.06 treatment significantly increased NK, T, and DC cell infiltration, but had little effect on macrophages (Figure 5B). Furthermore, while CD4 or CD8 T cell depletion with anti-CD4 or CD8b antibodies had only moderate effect on the IGSF8.06 antibody efficacy *in vivo* (Figures 5C and S6B), NK cell depletion with an anti-NK1.1 antibody completely abolished IGSF8.06 *in vivo* efficacy (Figure 5D). Since this antibody does not have Fc-mediated effector functions in mice, these results indicate that the blocking function of the IGSF8.06 antibody to activate NK cells is critical for the observed *in vivo* anti-tumor activity.

We further evaluated the *in vivo* efficacy of IGSF8.06 as a single agent or in combination with anti-PD1 in melanoma (B16-F10), Lewis lung carcinoma (LLC), colon cancer (CT26), and triple negative breast cancer (EMT6) syngeneic tumor models. In all the models, IGSF8.06 monotherapy demonstrated significant anti-tumor activity *in vivo* (Figures 5E and S6C–S6E). In addition, when we combined the two antibodies at half the dose of each, the efficacy exceeded either monotherapy at the full dose in all the models. Notably the B16-F10 model, with slightly lower MHC-I (and MHC-I defects[35]) and higher IGSF8 expression compared to the other models (Figures S6F and S6G), not only gave the best monotherapy efficacy *in vivo*, but also showed the best survival benefits from the combination treatment (Figure 5F). RNA-seq analyses of the syngeneic tumors revealed that IGSF8.06 treatment increased NK cell-mediated cytotoxicity, antigen processing and presentation, cell adhesion molecules, and T cell signaling (Figures S6H–S6K). Together, our results indicate that anti-IGSF8 antibody blocks the interaction between IGSF8 and its NK receptors, activates innate immunity, boosts antigen presentation, inhibits tumor growth in an NK cell-dependent manner, and has an additive effect with anti-PD1 treatment.

DISCUSSION

Antigen presentation defects are a well-known mechanism of tumor adaptive immune evasion and checkpoint inhibitor resistance, but the missing-self hypothesis posits that NK cells should eliminate malignant cells with MHC I defects.[61] Why NK cells fail to do this in tumors with antigen presentation defects has been poorly understood. Through CRISPR screens in malignant cells co-cultured with NK cells, we identified IGSF8, a previously undiscovered NK-cell checkpoint that is highly expressed on malignant cells to suppress NK-cell mediated cytotoxicity.

The results of any NK cell co-culture CRISPR screens are influenced by the type and state of NK cells used, the expression of HLA genes or other NK-cell modulators on the malignant cells, and other CRISPR screen conditions. We used both flow cytometry-based RNA-seq and CRISPR screens to identify the specific binding partner of IGSF8 on NK cells as KIR3DL2 in humans and Klra9 in mice. Through additional independent functional experiments, we demonstrated that IGSF8 binding to KIR3DL2, or Klra9 on NK cells inhibits the ability of NK cells to kill malignant cells. Despite having distinct evolutionary origins, human KIR3DL2 and mouse Klra9 are functional analogs, both serving as MHC-I receptors.[40,62] This suggests that an evolutionarily conserved function of IGSF8 to substitute for the presence of functional MHC-I is exploited by tumors with defective antigen presentation to suppress NK-cell killing. Through analysis of tumor single-cell data and immunohistochemistry staining, we observed that MHC-I and IGSF8 exhibit opposite expression patterns at both the mRNA and protein levels. However, there is no direct regulatory relationship between these two factors at the cellular level (Figures S1F–S1I), so we hypothesize that malignant cells with lower MHC-I are selected for higher IGSF8 expression by NK cells within the tumor microenvironment due to suppression of NK cell killing.

KIR3DL2 has been reported to bind to specific HLA alleles: HLA-A3, HLA-A11, HLA-B27, and HLA-F.[59,63–66] However, the high frequency of tumor MHC-I defects suggests that the

Please cite this article in press as: Li et al., IGSF8 is an innate immune checkpoint and cancer immunotherapy target, Cell (2024), https://doi.org/10.1016/j.cell.2024.03.039

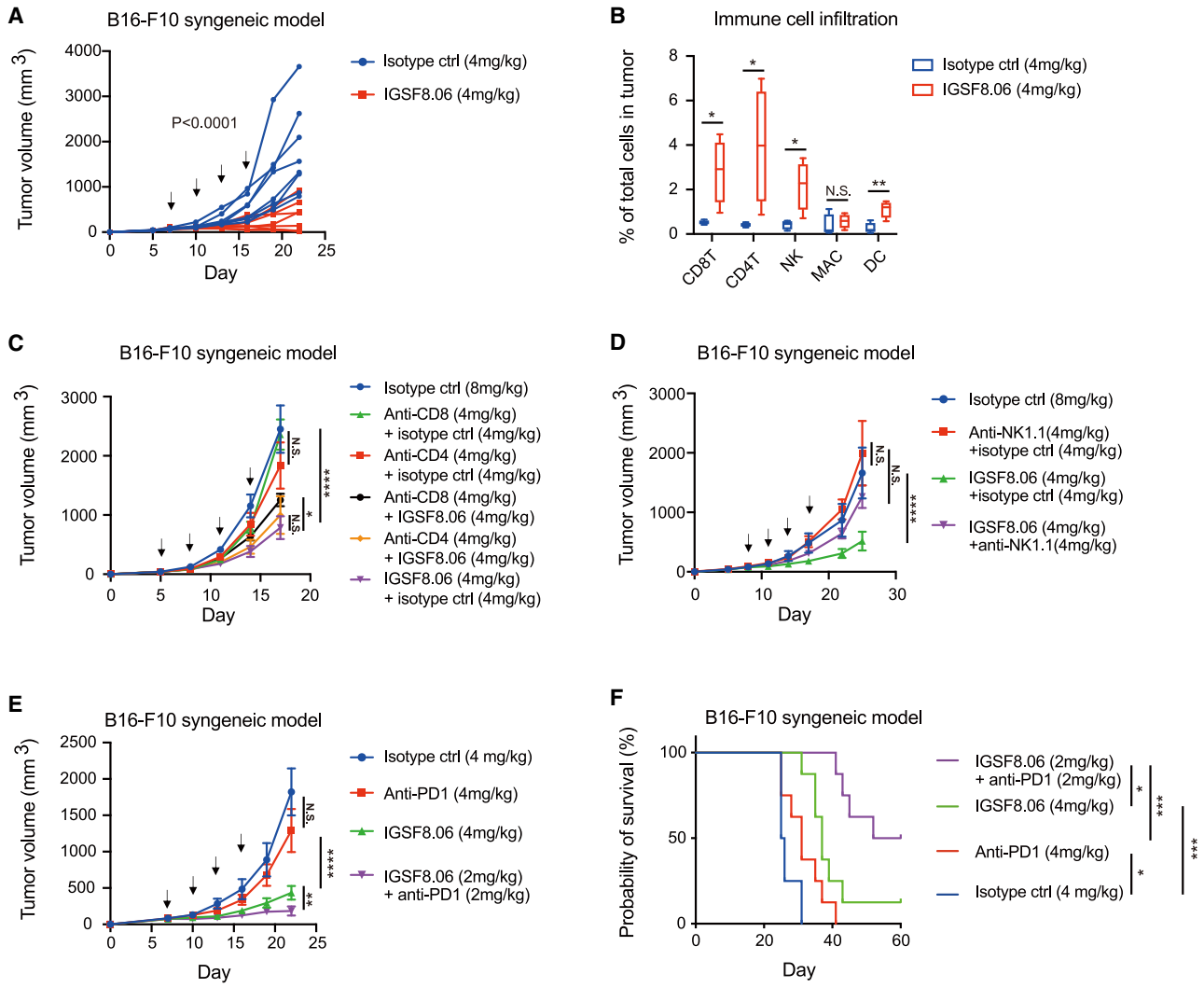

Figure 5. Igsf8 blockade by IGSF8.06 promotes anti-tumor immunity *in vivo*

(A) Monotherapy treatment of B16-F10 syngeneic model with control antibody (blue) and IGSF8.06 (red) ($n = 8$). The arrows indicate four administrations given to each group of mice on day 7, 10, 13, and 16.

(B) Flow cytometry of immune cell infiltration in B16-F10 tumors, as in Figure 1I. Mean ± SD ($n = 4$; two-tailed Student's t test; $^*p < 0.05$, $^{**}p < 0.01$) is plotted. DC indicates $CD11c^+$ $F4/80^-$ dendritic cells.

(C) Effects of CD4 or CD8 cell depletion by anti-CD4 or CD8b in B16-F10 syngeneic model treated with either IGSF8.06 or isotype controls ($n = 7$). The arrows indicate four administrations given to each group of mice on day 5, 8, 11, and 14.

(D) Effects of NK cell depletion by anti-NK1.1 in B16-F10 syngeneic model treated with either IGSF8.06 or isotype controls ($n = 8$). The arrows indicate four administrations given to each group of mice on day 8, 11, 14, and 17.

(E) B16-F10 syngeneic model treated with anti-PD1, IGSF8.06, combination, and isotype-matched controls at the dose and time (arrows) indicated ($n = 8$).

(F) Survival of B16-F10 syngeneic mice comparing anti-PD1, IGSF8.06, combination and control antibody treatment ($n = 8$). Data are represented as mean ± SEM unless otherwise noted. Statistics: a two-way ANOVA test with Greenhouse-Geisser correction was used to calculate significance (A and C–E); Log rank (Mantel-Cox) test (F). $^*p < 0.05$, $^{**}p < 0.01$, $^{***}p < 0.005$, $^{****}p < 0.001$. See also Figure S6.

previously known MHC-I ligands are unlikely KIR3DL2 interaction partners in tumors. In support of this hypothesis, although the *KIR3DL2* gene is present in all individuals,[67] its known MHC-I ligands are polymorphic and not expressed in all individuals. Among known ligands, KIR3DL2 binding to HLA-A3 and HLA-A11 is peptide specific,[68] and the A3/A11 epitope contributes little to education of KIR3DL2 positive NK cells.[69,70] KIR3DL2 binding to HLA-B27 is restricted to homodimers of HLA-B27 but not B2M-associated HLA-B27.[65] HLA-F expression is reported to be mostly restricted to the cytoplasm,[71] and cell surface expression of HLA-F has only been reported on activated immune cells[72] but not on malignant cells (Figure S1G). In contrast, *IGSF8* is an evolutionarily conserved gene with frequent copy number amplification and overexpression in tumors, making it a much more likely KIR3DL2 interaction partner in tumors. We also experimentally confirmed that IGSF8 can bind

to at least nine different KIR3DL2 variants (Figure 3H), covering 88.5% of tumor samples in the TCGA database, indicating that IGSF8-KIR3DL2 interaction is independent of common KIR3DL2 polymorphisms. Further studies are required to determine the impact of IGSF8.06 antibody blocking on the status of KIR3DL2 and the precise interaction sites between KIR3DL2 and IGSF8. KIR3DL2 is significantly upregulated in Sézary syndrome, and a clinical-stage anti-KIR3DL2 antibody Lacutamab was developed to deplete the malignant T cells as a treatment.[73] We note that Lacutamab does not block KIR3DL2 interaction with IGSF8 (Figure S2F). If IGSF8-KIR3DL2 interaction is also involved in Sézary syndrome, then an antibody targeting the ligand IGSF8 might be an alternative approach to treat this cancer. Therefore, evaluating the IGSF8-KIR3DL2 axis and anti-IGSF8 effect on Sézary syndrome will be of great interest and has the potential for rapid translation to the clinic.

The evidence presented here indicates that IGSF8 is an NK-cell checkpoint, but IGSF8 may have additional cancer-cell-intrinsic and -extrinsic functions, and other cell types may be involved in the IGSF8-mediated tumor immune evasion. First, IGSF8.06 antibody caused up-regulation of genes involved in antigen presentation and processing, which could in turn activate T cells. This is consistent with our *in vivo* observation (Figures S6H–S6K) and results of CD4/CD8 depletion experiments (Figure 5C), which support a function for T cells in the control of tumor growth by IGSF8.06 antibody *in vivo*. Second, although KIR3DL2 was known to be expressed on NK cells (Figure 3B), it is even more highly expressed on $\gamma\delta$ T cells in colorectal tumors (Figure 3D),[47,52] suggesting that IGSF8.06 antibody might activate $\gamma\delta$ T cells in these tumors. Third, IGSF8 also interacts with myeloid cells and may have different binding partners in these cells, including cell adhesion molecules CDH1 and CDH2 and myeloid-specific genes CLEC4A, CSF2RA, and MRC1 as potential IGSF8 binding partners.[38] This is consistent with our observation that syngeneic tumors treated with IGSF8.06 antibody exhibited increased expression of cell adhesion molecules and higher levels of dendritic cells (myeloid lineage) (Figures 5B and S6H–S6K). Fourth, single-cell analyses indicate that although IGSF8 is highly expressed in malignant cells, it is also expressed on some immune cells such as T cells, plasma cells, and DCs (Figure 3B). Therefore, IGSF8.06 antibody might have effects by binding directly to IGSF8 on immune cells. Further studies are required to fully elucidate the function of IGSF8 and understand the mechanism of IGSF8.06 antibody effects.

Previously developed antibodies against NK receptors have not delivered satisfactory clinical benefits, sowing doubt on the clinical promise of NK cell checkpoint inhibitors. We developed the IGSF8.06 antibody against evolutionarily conserved *IGSF8* expressed on malignant cells specifically to block IGSF8 interactions with NK cells. This antibody is unique in that it stimulates NK cells to kill malignant cells with antigen presentation defects and stress signals but spares normal cells that display normal MHC-I and no stress signals. Given the prevalence of human tumors with antigen presentation defects, IGSF8.06 antibody could have a potential to treat these immune-cold tumors by re-activating NK cells to kill malignant cells. This antibody might also be useful to prevent tumors that initially respond to anti-PD1 or anti-PD-L1 antibodies from developing resistance through antigen presentation loss. The dual targeting of T cells through PD1/PD-L1 and NK cells through IGSF8/KIR3DL2 might deliver the best efficacy and reduce the emergence of resistance to immunotherapy. The IGSF8.06 antibody did not exhibit significant toxicity in the mouse syngeneic tumors efficacy studies or in toxicology studies in rats and monkeys. No significant adverse effects or safety concerns were noted in animal studies even at drug dose of 80 mg/kg. We are currently investigating the safety and clinical activity of anti-IGSF8 as a cancer immunotherapy in a phase I clinical study in cancer patients (NCT05669430).

Limitations of the study

First, we could not obtain fresh tumor or normal tissues, so could not systematically evaluate IGSF8 and KIR3DL2 protein expression in different tissues or cell types. Second, we did not have enough syngeneic tumors with complete response to anti-IGSF8 treatment to conduct a tumor rechallenge experiment to evaluate whether the treatment leads to immunological memory and long-term protection. Third, immune checkpoints are inherently complex with pleiotropic functions, so it is likely that this study does not fully describe the function of IGSF8. Nevertheless, this study reveals a mechanism by which tumors upregulate IGSF8 to mimic MHC-I expression and thereby evade innate immunity and suggests antibody blockade of IGSF8 as a potentially effective cancer immunotherapeutic approach.

STAR★METHODS

Detailed methods are provided in the online version of this paper and include the following:

- KEY RESOURCES TABLE
- RESOURCE AVAILABILITY
  - Lead contact
  - Materials availability
  - Data and code availability
- EXPERIMENTAL MODEL AND STUDY PARTICIPANT DETAILS
  - Cancer cell culture
  - Primary NK culture
  - Primary NK cell expansion
  - Syngeneic tumor studies
- METHOD DETAILS
  - CRISPR screens
  - Deorphaning the IGSF8 receptor on NK cells by differential RNA-seq
  - Cell binding and blocking assays
  - *Ex vivo* mouse leukocyte profiling
  - Lentivirus production and purification
  - Gene essentiality in cell lines
  - Human and mouse NK cytotoxicity assay
  - Multiplexed immunohistochemistry staining
  - Surface plasmon resonance
  - Antibody discovery for IGSF8
  - Gene knockout by CRISPR
  - Gene overexpression by lentiviral particles
  - Recombinant protein and antibody expression and quality control
- QUANTIFICATION AND STATISTICAL ANALYSIS
  - CRISPR screening data analyzed by the MAGeCK algorithm
  - Statistics and survival analysis
  - Analysis of public scRNA-seq datasets
  - Structural similarities between MHC-I and IGSF8

Please cite this article in press as: Li et al., IGSF8 is an innate immune checkpoint and cancer immunotherapy target, Cell (2024), https://doi.org/10.1016/j.cell.2024.03.039

SUPPLEMENTAL INFORMATION

Supplemental information can be found online at https://doi.org/10.1016/j.cell.2024.03.039.

ACKNOWLEDGMENTS

We thank Drs. Lewis Lanier, Gordon Freeman, Myles Brown, Wayne Yokoyama, Jun Liu, and Kai Li for their helpful discussions. We also thank investors of GV20 Therapeutics for their financial support and all members of GV20 Therapeutics for their hard work to make this study a possibility.

AUTHOR CONTRIBUTIONS

X.H. X.S.L. and T.X. designed the study. Y.L., X.W., Hailing Liu, Huizhu Liu, Y.T., C.L., B.X., X.X., Q.Y., Z.G., J.G., M.T., W.W., J.Z., L.J., M.G., S.S., and G.Y. performed all experiments. X.H. and T.X. designed antibodies. C.S., Q.D., R.Z., J.M., J.W., M.P., and X.H. developed the algorithm and performed the analyses. W.Y., S.L., and X.B. helped with technical clarifications and result interpretations. X.H., X.S.L., and T.X. wrote the manuscript. All the authors participated in discussions and manuscript revision.

DECLARATION OF INTERESTS

All of the authors are current or former employees of GV20 Therapeutics, which develop drugs and research models for profit.

Received: August 10, 2023
Revised: December 18, 2023
Accepted: March 26, 2024
Published: April 23, 2024

REFERENCES

1. Haslam, A., and Prasad, V. (2019). Estimation of the Percentage of US Patients With Cancer Who Are Eligible for and Respond to Checkpoint Inhibitor Immunotherapy Drugs. JAMA Netw. Open *2*, e192535.
2. Gajewski, T.F., Schreiber, H., and Fu, Y.-X. (2013). Innate and adaptive immune cells in the tumor microenvironment. Nat. Immunol. *14*, 1014–1022.
3. Jiang, P., Gu, S., Pan, D., Fu, J., Sahu, A., Hu, X., Li, Z., Traugh, N., Bu, X., Li, B., et al. (2018). Signatures of T cell dysfunction and exclusion predict cancer immunotherapy response. Nat. Med. *24*, 1550–1558.
4. Pauken, K.E., Sammons, M.A., Odorizzi, P.M., Manne, S., Godec, J., Khan, O., Drake, A.M., Chen, Z., Sen, D.R., Kurachi, M., et al. (2016). Epigenetic stability of exhausted T cells limits durability of reinvigoration by PD-1 blockade. Science *354*, 1160–1165.
5. Philip, M., Fairchild, L., Sun, L., Horste, E.L., Camara, S., Shakiba, M., Scott, A.C., Viale, A., Lauer, P., Merghoub, T., et al. (2017). Chromatin states define tumour-specific T cell dysfunction and reprogramming. Nature *545*, 452–456.
6. Zaretsky, J.M., Garcia-Diaz, A., Shin, D.S., Escuin-Ordinas, H., Hugo, W., Hu-Lieskovan, S., Torrejon, D.Y., Abril-Rodriguez, G., Sandoval, S., Barthly, L., et al. (2016). Mutations Associated with Acquired Resistance to PD-1 Blockade in Melanoma. N. Engl. J. Med. *375*, 819–829.
7. Sade-Feldman, M., Jiao, Y.J., Chen, J.H., Rooney, M.S., Barzily-Rokni, M., Eliane, J.-P., Bjorgaard, S.L., Hammond, M.R., Vitzthum, H., Blackmon, S.M., et al. (2017). Resistance to checkpoint blockade therapy through inactivation of antigen presentation. Nat. Commun. *8*, 1136.
8. Garrido, F., Aptsiauri, N., Doorduijn, E.M., Garcia Lora, A.M., and van Hall, T. (2016). The urgent need to recover MHC class I in cancers for effective immunotherapy. Curr. Opin. Immunol. *39*, 44–51.
9. Cornel, A.M., Mimpen, I.L., and Nierkens, S. (2020). MHC Class I Downregulation in Cancer: Underlying Mechanisms and Potential Targets for Cancer Immunotherapy. Cancers *12*, 1760. https://doi.org/10.3390/cancers12071760.
10. Burr, M.L., Sparbier, C.E., Chan, K.L., Chan, Y.-C., Kersbergen, A., Lam, E.Y.N., Azidis-Yates, E., Vassiliadis, D., Bell, C.C., Gilan, O., et al. (2019). An Evolutionarily Conserved Function of Polycomb Silences the MHC Class I Antigen Presentation Pathway and Enables Immune Evasion in Cancer. Cancer Cell *36*, 385–401.e8.
11. Yamamoto, K., Venida, A., Yano, J., Biancur, D.E., Kakiuchi, M., Gupta, S., Sohn, A.S.W., Mukhopadhyay, S., Lin, E.Y., Parker, S.J., et al. (2020). Autophagy promotes immune evasion of pancreatic cancer by degrading MHC-I. Nature *581*, 100–105.
12. Vivier, E., Raulet, D.H., Moretta, A., Caligiuri, M.A., Zitvogel, L., Lanier, L.L., Yokoyama, W.M., and Ugolini, S. (2011). Innate or adaptive immunity? The example of natural killer cells. Science *331*, 44–49.
13. Abril, E., Mendez, R.E., García, A., Serrano, A., Cabrera, T., Garrido, F., and Ruiz-Cabello, F. (1996). Characterization of a gastric tumor cell line defective in MHC class I inducibility by both alpha- and gamma-interferon. Tissue Antigens *47*, 391–398.
14. Li, W., Xu, H., Xiao, T., Cong, L., Love, M.I., Zhang, F., Irizarry, R.A., Liu, J.S., Brown, M., and Liu, X.S. (2014). MAGeCK enables robust identification of essential genes from genome-scale CRISPR/Cas9 knockout screens. Genome Biol. *15*, 554.
15. Pende, D., Falco, M., Vitale, M., Cantoni, C., Vitale, C., Munari, E., Bertaina, A., Moretta, F., Del Zotto, G., Pietra, G., et al. (2019). Killer Ig-Like Receptors (KIRs): Their Role in NK Cell Modulation and Developments Leading to Their Clinical Exploitation. Front. Immunol. *10*, 1179.
16. Kaiser, B.K., Pizarro, J.C., Kerns, J., and Strong, R.K. (2008). Structural basis for NKG2A/CD94 recognition of HLA-E. Proc. Natl. Acad. Sci. USA *105*, 6696–6701.
17. Park, D.J., Sung, P.S., Kim, J.-H., Lee, G.W., Jang, J.W., Jung, E.S., Bae, S.H., Choi, J.Y., and Yoon, S.K. (2020). EpCAM-high liver cancer stem cells resist natural killer cell-mediated cytotoxicity by upregulating CEACAM1. J. Immunother. Cancer *8*, e000301. https://doi.org/10.1136/jitc-2019-000301.
18. Wu, H.-T., and Zhao, X.-Y. (2022). Regulation of CD38 on Multiple Myeloma and NK Cells by Monoclonal Antibodies. Int. J. Biol. Sci. *18*, 1974–1988.
19. Stanietsky, N., Simic, H., Arapovic, J., Toporik, A., Levy, O., Novik, A., Levine, Z., Beiman, M., Dassa, L., Achdout, H., et al. (2009). The interaction of TIGIT with PVR and PVRL2 inhibits human NK cell cytotoxicity. Proc. Natl. Acad. Sci. USA *106*, 17858–17863.
20. Ren, X., Peng, M., Xing, P., Wei, Y., Galbo, P.M., Jr., Corrigan, D., Wang, H., Su, Y., Dong, X., Sun, Q., et al. (2022). Blockade of the immunosuppressive KIR2DL5/PVR pathway elicits potent human NK cell-mediated antitumor immunity. J. Clin. Invest. *132*, e163620. https://doi.org/10.1172/JCI163620.
21. Brandt, C.S., Baratin, M., Yi, E.C., Kennedy, J., Gao, Z., Fox, B., Haldeman, B., Ostrander, C.D., Kaifu, T., Chabannon, C., et al. (2009). The B7 family member B7-H6 is a tumor cell ligand for the activating natural killer cell receptor NKp30 in humans. J. Exp. Med. *206*, 1495–1503.
22. Wang, R., Jaw, J.J., Stutzman, N.C., Zou, Z., and Sun, P.D. (2012). Natural killer cell-produced IFN-γ and TNF-α induce target cell cytolysis through up-regulation of ICAM-1. J. Leukoc. Biol. *91*, 299–309.
23. Steinle, A., Li, P., Morris, D.L., Groh, V., Lanier, L.L., Strong, R.K., and Spies, T. (2001). Interactions of human NKG2D with its ligands MICA, MICB, and homologs of the mouse RAE-1 protein family. Immunogenetics *53*, 279–287.
24. Zhang, Y., Liu, Q., Yang, S., and Liao, Q. (2021). CD58 Immunobiology at a Glance. Front. Immunol. *12*, 705260.
25. Zhuang, X., Veltri, D.P., and Long, E.O. (2019). Genome-Wide CRISPR Screen Reveals Cancer Cell Resistance to NK Cells Induced by NK-Derived IFN-γ. Front. Immunol. *10*, 2879.
26. Ray, A., and Treloar, H.B. (2012). IgSF8: a developmentally and functionally regulated cell adhesion molecule in olfactory sensory neuron axons and synapses. Mol. Cell. Neurosci. *50*, 238–249.

27. Zhang, X.A., Lane, W.S., Charrin, S., Rubinstein, E., and Liu, L. (2003). EWI2/PGRL associates with the metastasis suppressor KAI1/CD82 and inhibits the migration of prostate malignant cells. Cancer Res. *63*, 2665–2674.

28. Montpellier, C., Tews, B.A., Poitrimole, J., Rocha-Perugini, V., D'Arienzo, V., Potel, J., Zhang, X.A., Rubinstein, E., Dubuisson, J., and Cocquerel, L. (2011). Interacting regions of CD81 and two of its partners, EWI-2 and EWI-2wint, and their effect on hepatitis C virus infection. J. Biol. Chem. *286*, 13954–13965.

29. Gordón-Alonso, M., Sala-Valdés, M., Rocha-Perugini, V., Pérez-Hernández, D., López-Martín, S., Ursa, A., Alvarez, S., Kolesnikova, T.V., Vázquez, J., Sánchez-Madrid, F., and Yáñez-Mó, M. (2012). EWI-2 association with α-actinin regulates T cell immune synapses and HIV viral infection. J. Immunol. *189*, 689–700.

30. Kolesnikova, T.V., Kazarov, A.R., Lemieux, M.E., Lafleur, M.A., Kesari, S., Kung, A.L., and Hemler, M.E. (2009). Glioblastoma inhibition by cell surface immunoglobulin protein EWI-2, in vitro and in vivo. Neoplasia *11*, 77–86. 4p following 86.

31. Ghandi, M., Huang, F.W., Jané-Valbuena, J., Kryukov, G.V., Lo, C.C., McDonald, E.R., 3rd, Barretina, J., Gelfand, E.T., Bielski, C.M., Li, H., et al. (2019). Next-generation characterization of the Cancer Cell Line Encyclopedia. Nature *569*, 503–508.

32. Gu, S.S., Zhang, W., Wang, X., Jiang, P., Traugh, N., Li, Z., Meyer, C., Stewig, B., Xie, Y., Bu, X., et al. (2021). Therapeutically Increasing MHC-I Expression Potentiates Immune Checkpoint Blockade. Cancer Discov. *11*, 1524–1541.

33. Alter, G., Malenfant, J.M., and Altfeld, M. (2004). CD107a as a functional marker for the identification of natural killer cell activity. J. Immunol. Methods *294*, 15–22.

34. Kearney, C.J., Vervoort, S.J., Hogg, S.J., Ramsbottom, K.M., Freeman, A.J., Lalaoui, N., Pijpers, L., Michie, J., Brown, K.K., Knight, D.A., et al. (2018). Tumor immune evasion arises through loss of TNF sensitivity. Sci. Immunol. *3*, eaar3451. https://doi.org/10.1126/sciimmunol.aar3451.

35. Seliger, B., Wollscheid, U., Momburg, F., Blankenstein, T., and Huber, C. (2001). Characterization of the major histocompatibility complex class I deficiencies in B16 melanoma cells. Cancer Res. *61*, 1095–1099.

36. Freeman, A.J., Vervoort, S.J., Ramsbottom, K.M., Kelly, M.J., Michie, J., Pijpers, L., Johnstone, R.W., Kearney, C.J., and Oliaro, J. (2019). Natural Killer Cells Suppress T Cell-Associated Tumor Immune Evasion. Cell Rep. *28*, 2784–2794.e5.

37. Anfossi, N., André, P., Guia, S., Falk, C.S., Roetynck, S., Stewart, C.A., Breso, V., Frassati, C., Reviron, D., Middleton, D., et al. (2006). Human NK cell education by inhibitory receptors for MHC class I. Immunity *25*, 331–342.

38. Shilts, J., Severin, Y., Galaway, F., Müller-Sienerth, N., Chong, Z.-S., Pritchard, S., Teichmann, S., Vento-Tormo, R., Snijder, B., and Wright, G.J. (2022). A physical wiring diagram for the human immune system. Nature *608*, 397–404.

39. Hamerman, J.A., Ogasawara, K., and Lanier, L.L. (2005). NK cells in innate immunity. Curr. Opin. Immunol. *17*, 29–35.

40. Shaw, J., and Kollnberger, S. (2012). New perspectives on the ligands and function of the killer cell immunoglobulin-like receptor KIR3DL2 in health and disease. Front. Immunol. *3*, 339.

41. Proteau, M.-F., Rousselle, E., and Makrigiannis, A.P. (2004). Mapping of the BALB/c Ly49 cluster defines a minimal natural killer cell receptor gene repertoire. Genomics *84*, 669–677.

42. Fabry, Z., Raine, C.S., and Hart, M.N. (1994). Nervous tissue as an immune compartment: the dialect of the immune response in the CNS. Immunol. Today Off. *15*, 218–224.

43. Lampson, L.A. (1995). Interpreting MHC class I expression and class I/class II reciprocity in the CNS: reconciling divergent findings. Microsc. Res. Tech. *32*, 267–285.

44. Aloisi, F., Ria, F., and Adorini, L. (2000). Regulation of T-cell responses by CNS antigen-presenting cells: different roles for microglia and astrocytes. Immunol. Today Off. *21*, 141–147.

45. Hickey, W.F. (2001). Basic principles of immunological surveillance of the normal central nervous system. Glia *36*, 118–124.

46. Han, Y., Wang, Y., Dong, X., Sun, D., Liu, Z., Yue, J., Wang, H., Li, T., and Wang, C. (2023). TISCH2: expanded datasets and new tools for single-cell transcriptome analyses of the tumor microenvironment. Nucleic Acids Res. *51*, D1425–D1431.

47. Pelka, K., Hofree, M., Chen, J.H., Sarkizova, S., Pirl, J.D., Jorgji, V., Bejnood, A., Dionne, D., Ge, W.H., Xu, K.H., et al. (2021). Spatially organized multicellular immune hubs in human colorectal cancer. Cell *184*, 4734–4752.e20.

48. Riaz, N., Havel, J.J., Makarov, V., Desrichard, A., Urba, W.J., Sims, J.S., Hodi, F.S., Martín-Algarra, S., Mandal, R., Sharfman, W.H., et al. (2017). Tumor and Microenvironment Evolution during Immunotherapy with Nivolumab. Cell *171*, 934–949.e16.

49. Burr, M.L., van den Boomen, D.J.H., Bye, H., Antrobus, R., Wiertz, E.J., and Lehner, P.J. (2013). MHC class I molecules are preferentially ubiquitinated on endoplasmic reticulum luminal residues during HRD1 ubiquitin E3 ligase-mediated dislocation. Proc. Natl. Acad. Sci. USA *110*, 14290–14295.

50. van den Boomen, D.J.H., Timms, R.T., Grice, G.L., Stagg, H.R., Skødt, K., Dougan, G., Nathan, J.A., and Lehner, P.J. (2014). TMEM129 is a Derlin-1 associated ERAD E3 ligase essential for virus-induced degradation of MHC-I. Proc. Natl. Acad. Sci. USA *111*, 11425–11430.

51. Wang, Y., Wang, X., Cui, X., Zhuo, Y., Li, H., Ha, C., Xin, L., Ren, Y., Zhang, W., Sun, X., et al. (2020). Oncoprotein SND1 hijacks nascent MHC-I heavy chain to ER-associated degradation, leading to impaired CD8 T cell response in tumor. Sci. Adv. *6*, eaba5412. https://doi.org/10.1126/sciadv.aba5412.

52. de Vries, N.L., van de Haar, J., Veninga, V., Chalabi, M., Ijsselsteijn, M.E., van der Ploeg, M., van den Bulk, J., Ruano, D., van den Berg, J.G., Haanen, J.B., et al. (2023). γδ T cells are effectors of immunotherapy in cancers with HLA class I defects. Nature *613*, 743–750.

53. Xu, W., Atkins, M.B., and McDermott, D.F. (2020). Checkpoint inhibitor immunotherapy in kidney cancer. Nat. Rev. Urol. *17*, 137–150.

54. Mertins, P., Mani, D.R., Ruggles, K.V., Gillette, M.A., Clauser, K.R., Wang, P., Wang, X., Qiao, J.W., Cao, S., Petralia, F., et al. (2016). Proteogenomics connects somatic mutations to signalling in breast cancer. Nature *534*, 55–62.

55. Zhang, H., Liu, T., Zhang, Z., Payne, S.H., Zhang, B., McDermott, J.E., Zhou, J.-Y., Petyuk, V.A., Chen, L., Ray, D., et al. (2016). Integrated Proteogenomic Characterization of Human High-Grade Serous Ovarian Cancer. Cell *166*, 755–765.

56. Hugo, W., Zaretsky, J.M., Sun, L., Song, C., Moreno, B.H., Hu-Lieskovan, S., Berent-Maoz, B., Pang, J., Chmielowski, B., Cherry, G., et al. (2016). Genomic and Transcriptomic Features of Response to Anti-PD-1 Therapy in Metastatic Melanoma. Cell *165*, 35–44.

57. Amorim, L.M., Augusto, D.G., Nemat-Gorgani, N., Montero-Martin, G., Marin, W.M., Shams, H., Dandekar, R., Caillier, S., Parham, P., Fernández-Viña, M.A., et al. (2021). High-Resolution Characterization of Genes in a Large North American Cohort Reveals Novel Details of Structural and Sequence Diversity. Front. Immunol. *12*, 674778.

58. Song, L., Bai, G., Liu, X.S., Li, B., and Li, H. (2023). Efficient and accurate KIR and HLA genotyping with massively parallel sequencing data. Genome Res. *33*, 923–931.

59. Pende, D., Biassoni, R., Cantoni, C., Verdiani, S., Falco, M., di Donato, C., Accame, L., Bottino, C., Moretta, A., and Moretta, L. (1996). The natural killer cell receptor specific for HLA-A allotypes: a novel member of the p58/p70 family of inhibitory receptors that is characterized by three immunoglobulin-like domains and is expressed as a 140-kD disulphide-linked dimer. J. Exp. Med. *184*, 505–518.

60. Blake, J.A., Baldarelli, R., Kadin, J.A., Richardson, J.E., Smith, C.L., and Bult, C.J.; Mouse Genome Database Group (2021). Mouse Genome Database (MGD): Knowledgebase for mouse-human comparative biology. Nucleic Acids Res. *49*, D981–D987.

61. Ljunggren, H.G., and Kärre, K. (1990). In search of the "missing self": MHC molecules and NK cell recognition. Immunol. Today *11*, 237–244.

62. Schenkel, A.R., Kingry, L.C., and Slayden, R.A. (2013). The ly49 gene family. A brief guide to the nomenclature, genetics, and role in intracellular infection. Front. Immunol. *4*, 90.

63. Wagtmann, N., Biassoni, R., Cantoni, C., Verdiani, S., Malnati, M.S., Vitale, M., Bottino, C., Moretta, L., Moretta, A., and Long, E.O. (1995). Molecular clones of the p58 NK cell receptor reveal immunoglobulin-related molecules with diversity in both the extra- and intracellular domains. Immunity *2*, 439–449.

64. Döhring, C., Scheidegger, D., Samaridis, J., Cella, M., and Colonna, M. (1996). A human killer inhibitory receptor specific for HLA-A1,2. J. Immunol. *156*, 3098–3101.

65. Wong-Baeza, I., Ridley, A., Shaw, J., Hatano, H., Rysnik, O., McHugh, K., Piper, C., Brackenbridge, S., Fernandes, R., Chan, A., et al. (2013). KIR3DL2 binds to HLA-B27 dimers and free H chains more strongly than other HLA class I and promotes the expansion of T cells in ankylosing spondylitis. J. Immunol. *190*, 3216–3224.

66. Goodridge, J.P., Burian, A., Lee, N., and Geraghty, D.E. (2013). HLA-F and MHC class I open conformers are ligands for NK cell Ig-like receptors. J. Immunol. *191*, 3553–3562.

67. Schmitt, C., Marie-Cardine, A., and Bensussan, A. (2017). Therapeutic Antibodies to KIR3DL2 and Other Target Antigens on Cutaneous T-Cell Lymphomas. Front. Immunol. *8*, 1010.

68. Hansasuta, P., Dong, T., Thananchai, H., Weekes, M., Willberg, C., Aldemir, H., Rowland-Jones, S., and Braud, V.M. (2004). Recognition of HLA-A3 and HLA-A11 by KIR3DL2 is peptide-specific. Eur. J. Immunol. *34*, 1673–1679.

69. Yawata, M., Yawata, N., Draghi, M., Partheniou, F., Little, A.-M., and Parham, P. (2008). MHC class I-specific inhibitory receptors and their ligands structure diverse human NK-cell repertoires toward a balance of missing self-response. Blood *112*, 2369–2380.

70. Fauriat, C., Andersson, S., Björklund, A.T., Carlsten, M., Schaffer, M., Björkström, N.K., Baumann, B.C., Michaëlsson, J., Ljunggren, H.-G., and Malmberg, K.-J. (2008). Estimation of the size of the alloreactive NK cell repertoire: studies in individuals homozygous for the group A KIR haplotype. J. Immunol. *181*, 6010–6019.

71. Lepin, E.J., Bastin, J.M., Allan, D.S., Roncador, G., Braud, V.M., Mason, D.Y., van der Merwe, P.A., McMichael, A.J., Bell, J.I., Powis, S.H., and O'Callaghan, C.A. (2000). Functional characterization of HLA-F and binding of HLA-F tetramers to ILT2 and ILT4 receptors. Eur. J. Immunol. *30*, 3552–3561.

72. Lee, N., Ishitani, A., and Geraghty, D.E. (2010). HLA-F is a surface marker on activated lymphocytes. Eur. J. Immunol. *40*, 2308–2318.

73. Bagot, M., Porcu, P., Marie-Cardine, A., Battistella, M., William, B.M., Vermeer, M., Whittaker, S., Rotolo, F., Ram-Wolff, C., Khodadoust, M.S., et al. (2019). IPH4102, a first-in-class anti-KIR3DL2 monoclonal antibody, in patients with relapsed or refractory cutaneous T-cell lymphoma: an international, first-in-human, open-label, phase 1 trial. Lancet Oncol *20*, 1160–1170.

74. Liu, J., Lichtenberg, T., Hoadley, K.A., Poisson, L.M., Lazar, A.J., Cherniack, A.D., Kovatich, A.J., Benz, C.C., Levine, D.A., Lee, A.V., et al. (2018). An Integrated TCGA Pan-Cancer Clinical Data Resource to Drive High-Quality Survival Outcome Analytics. Cell *173*, 400–416.e11.

75. Yang, Y., Badeti, S., Tseng, H.-C., Ma, M.T., Liu, T., Jiang, J.-G., Liu, C., and Liu, D. (2020). Superior Expansion and Cytotoxicity of Human Primary NK and CAR-NK Cells from Various Sources via Enriched Metabolic Pathways. Mol. Ther. Methods Clin. Dev. *18*, 428–445.

76. Wolf, F.A., Angerer, P., and Theis, F.J. (2018). SCANPY: large-scale single-cell gene expression data analysis. Genome Biol. *19*, 15.

77. Jumper, J., Evans, R., Pritzel, A., Green, T., Figurnov, M., Ronneberger, O., Tunyasuvunakool, K., Bates, R., Žídek, A., Potapenko, A., et al. (2021). Highly accurate protein structure prediction with AlphaFold. Nature *596*, 583–589.

78. Zhang, C., Shine, M., Pyle, A.M., and Zhang, Y. (2022). US-align: universal structure alignments of proteins, nucleic acids, and macromolecular complexes. Nat. Methods *19*, 1109–1115.

79. Xu, H., Xiao, T., Chen, C.-H., Li, W., Meyer, C.A., Wu, Q., Wu, D., Cong, L., Zhang, F., Liu, J.S., et al. (2015). Sequence determinants of improved CRISPR sgRNA design. Genome Res. *25*, 1147–1157.

80. Sanjana, N.E., Shalem, O., and Zhang, F. (2014). Improved vectors and genome-wide libraries for CRISPR screening. Nat. Methods *11*, 783–784.

81. Xiao, T., Li, W., Wang, X., Xu, H., Yang, J., Wu, Q., Huang, Y., Geradts, J., Jiang, P., Fei, T., et al. (2018). Estrogen-regulated feedback loop limits the efficacy of estrogen receptor-targeted breast cancer therapy. Proc. Natl. Acad. Sci. USA *115*, 7869–7878.

82. Kandarian, F., Sunga, G.M., Arango-Saenz, D., and Rossetti, M. (2017). A Flow Cytometry-Based Cytotoxicity Assay for the Assessment of Human NK Cell Activity. J. Vis. Exp. 56191. https://doi.org/10.3791/56191.

83. Schlothauer, T., Herter, S., Koller, C.F., Grau-Richards, S., Steinhart, V., Spick, C., Kubbies, M., Klein, C., Umaña, P., and Mössner, E. (2016). Novel human IgG1 and IgG4 Fc-engineered antibodies with completely abolished immune effector functions. Protein Eng. Des. Sel. *29*, 457–466.

84. Umeda, R., Satouh, Y., Takemoto, M., Nakada-Nakura, Y., Liu, K., Yokoyama, T., Shirouzu, M., Iwata, S., Nomura, N., Sato, K., et al. (2020). Structural insights into tetraspanin CD9 function. Nat. Commun. *11*, 1606.

85. Grasso, C.S., Tsoi, J., Onyshchenko, M., Abril-Rodriguez, G., Ross-Macdonald, P., Wind-Rotolo, M., Champhekar, A., Medina, E., Torrejon, D.Y., Shin, D.S., et al. (2020). Conserved Interferon-γ Signaling Drives Clinical Response to Immune Checkpoint Blockade Therapy in Melanoma. Cancer Cell *38*, 500–515.e3.

Please cite this article in press as: Li et al., IGSF8 is an innate immune checkpoint and cancer immunotherapy target, Cell (2024), https://doi.org/10.1016/j.cell.2024.03.039

STAR★METHODS

KEY RESOURCES TABLE

REAGENT or RESOURCE	SOURCE	IDENTIFIER
Antibodies		
Anti-human PE-conjugated HLA-A,B,C (clone W6/32)	BioLegend	Cat# 311405; RRID: AB_314874
Anti-human PE/Dazzle-conjugated 594 HLA-E (clone 3D12)	BioLegend	Cat# 342615; RRID: AB_2814258
Anti-human PE-conjugated HLA-F (clone 3D11/HLA-F)	BioLegend	Cat# 373203; RRID:AB_2650871
Anti-human PE-conjugated HLA-G (clone 87G)	BioLegend	Cat# 335905; RRID:AB_1227710
Anti-human PE-conjugated CD3 (clone HIT3a)	BioLegend	Cat# 300308; RRID:AB_314044
Anti-human KIR3DL2/CD158k (clone #539304)	R&D systems	Cat# MAB2878; RRID:AB_3086694
Anti-human PE-conjugated CD56 (clone 5.1H11)	BioLegend	Cat# 362508; RRID:AB_2563925
Anti-human Alexa Fluor 700-conjugated CD56 (clone 5.1H11)	BioLegend	Cat# 362522; RRID:AB_2564099
Anti-human APC-conjugated CD56 (clone 5.1H11)	BioLegend	Cat# 362504; RRID:AB_2563913
Anti-human PE-conjugated IgG Fc (clone M1310G05)	BioLegend	Cat# 410708; RRID:AB_2565786
Anti-human APC-conjugated IgG Fc (clone M1310G05)	BioLegend	Cat# 410712; RRID:AB_2565790
Anti-human FITC-conjugated IgG Fc (clone M1310G05)	BioLegend	Cat# 410720; RRID:AB_2721576
Anti-human APC-conjugated Beta-2 microglobulin (Mouse IgG1 Clone #35)	SinoBiological	Cat# 11976-MM35-A; RRID: AB_3086735
Anti-IGSF8 Antibody, Rabbit Polyclonal	SinoBiological	Cat# 13435-T16; RRID: AB_3086693
Anti-IGSF8 antibody produced in rabbit	Sigma-Aldrich	Cat# HPA011917; RRID:AB_1851536
Anti-pan Cytokeratin (clone AE1/3)	Gene tech	Cat# GM351507; RRID: AB_3086695
Anti-human FITC-conjugated CD4 (clone RPA-T4)	BioLegend	Cat# 300506; RRID:AB_314074
Anti-human Pacific Blue-conjugated CD8 (clone SK1)	BioLegend	Cat# 344718; RRID:AB_10551438
Anti-human PE/Cyanine7-conjugated CD14 (clone 63D3)	BioLegend	Cat# 367112; RRID:AB_2566714
Anti-human APC-conjugated Perforin (clone dG9)	BioLegend	Cat# 308112; RRID:AB_2252843
Anti-human Brilliant Violet 421-conjugated IgG Fc (clone HP6017)	BioLegend	Cat# 409318; RRID:AB_2562176
Anti-human APC-conjugated CD107a (clone H4A3)	BioLegend	Cat# 328620; RRID:AB_1279055
Anti-human PE-conjugated CD85j (ILT2) (clone GHI/75)	BioLegend	Cat# 333708; RRID:AB_2136385
Anti-human APC-conjugated CD158b/j (KIR2DL2/L3/S2) (clone DX27)	BioLegend	Cat# 312612; RRID:AB_2563377
Anti-human APC-conjugated CD158e1 (KIR3DL1, NKB1) (clone DX9)	BioLegend	Cat# 312716; RRID:AB_2563360

(*Continued on next page*)

Please cite this article in press as: Li et al., IGSF8 is an innate immune checkpoint and cancer immunotherapy target, Cell (2024), https://doi.org/10.1016/j.cell.2024.03.039

Continued

REAGENT or RESOURCE	SOURCE	IDENTIFIER
Anti-human PD1 (CD279) (clone J116)	Bio X Cell	Cat# BE0188; RRID:AB_10950318
Human IgG1 isotype control	Bio X Cell	Cat# BE0297; RRID: AB_2687817
Anti-MHC class I + HLA A + HLA B antibody (clone EPR1394Y)	Abcam	Cat# ab134189; RRID:AB_3073854
Anti-mouse/human PE/Cyanine7-conjugated CD11b (clone M1/70)	BioLegend	Cat# 101216; RRID:AB_312799
Anti-mouse/human PerCP/Cyanine5.5-conjugated CD11b (clone M1/70)	BioLegend	Cat# 101228; RRID:AB_893232
Anti-mouse PerCP/Cyanine5.5-conjugated CD45 (clone I3/2.3)	BioLegend	Cat# 147706; RRID:AB_2563538
Anti-mouse PE/Cyanine7-conjugated CD45 (clone S18009F)	BioLegend	Cat# 157206; RRID:AB_2860726
Anti-mouse APC-conjugated CD19 (clone 6D5)	BioLegend	Cat# 115512; RRID:AB_313647
Anti-mouse Pacific Blue-conjugated CD19 (clone 6D5)	BioLegend	Cat# 115523; RRID:AB_439718
Anti-mouse PE/Cyanine7-conjugated CD19 (clone 6D5)	BioLegend	Cat# 115520; RRID:AB_313655
Anti-mouse PE-conjugated F4/80 (clone BM8)	BioLegend	Cat# 123110; RRID:AB_893486
Anti-mouse FITC-conjugated F4/80 (clone BM8)	BioLegend	Cat# 123108; RRID:AB_893502
Anti-mouse PE/Cyanine7-conjugated F4/80 (clone BM8)	BioLegend	Cat# 123114; RRID:AB_893478
Anti-mouse FITC-conjugated CD3 (clone 17A2)	BioLegend	Cat# 100204; RRID:AB_312661
Anti-mouse PerCP-conjugated CD11c (clone N418)	BioLegend	Cat# 117326; RRID:AB_2129643
Anti-mouse PE-conjugated CD11c (clone N418)	BioLegend	Cat# 117308; RRID:AB_313777
Anti-mouse Brilliant Violet 605-conjugated CD11c (clone N418)	BioLegend	Cat# 117334; RRID:AB_2562415
Anti-mouse FITC-conjugated CD11c (clone N418)	BioLegend	Cat# 117306; RRID:AB_313775
Anti-mouse Alexa Fluor 700-conjugated CD4 (clone GK1.5)	BioLegend	Cat# 100430; RRID:AB_493699
Anti-mouse Pacific Blue-conjugated CD8a (clone 53-6.7)	BioLegend	Cat# 100725; RRID:AB_493425
Anti-mouse APC-conjugated NK1.1 (clone PK136)	BioLegend	Cat# 108709; RRID:AB_313396
Anti-mouse PE-conjugated NK1.1 (clone PK136)	BioLegend	Cat# 108708; RRID:AB_313395
Anti-mouse PE-conjugated Ly-49I (clone YLI-90)	Thermo Fisher Scientific	Cat# 12-5895-82; RRID:AB_466021
Mouse IgG1 isotype control (clone MOPC-21)	Bio X Cell	Cat# BE0083; RRID:AB_1107784
Anti-mouse NK1.1 (clone PK136)	Bio X Cell	Cat# BE0036; RRID:AB_1107737
Anti-mouse CD8β (Lyt 3.2) (clone 53-5.8)	Bio X Cell	Cat# BE0223; RRID:AB_2687706
Anti-mouse CD4 (clone YTS 191)	Bio X Cell	Cat# BE0119; RRID:AB_10950382
Anti-mouse PD-1 (CD279) (clone 29F.1A12)	Bio X Cell	Cat# BE0273; RRID: AB_2687796
Mouse IgG2a isotype control (clone C1.18.4)	Bio X Cell	Cat# BE0085; RRID:AB_1107771

(*Continued on next page*)

Please cite this article in press as: Li et al., IGSF8 is an innate immune checkpoint and cancer immunotherapy target, Cell (2024), https://doi.org/10.1016/j.cell.2024.03.039

Continued

REAGENT or RESOURCE	SOURCE	IDENTIFIER
Anti-mouse FITC-conjugated IgG1 kappa Isotype Control (clone P3.6.2.8.1)	Thermo Fisher Scientific	Cat# 11-4714-42; RRID:AB_10596964
Anti-mouse PerCP-eFluor 710-conjugated IgG1 kappa Isotype Control (clone P3.6.2.8.1)	Thermo Fisher Scientific	Cat# 46-4714-82; RRID:AB_1834453
SuperBoost™ Goat anti-Mouse Poly HRP	Thermo Fisher Scientific	Cat# B40961; RRID:AB_3096292
SuperBoost™ Goat anti-Rabbit Poly HRP	Thermo Fisher Scientific	Cat# B40962; RRID:AB_3096294
PE-conjugated F(ab')2-Goat anti-Mouse IgG (H + L) Secondary Antibody	Thermo Fisher Scientific	Cat# 12-4010-82; RRID: AB_11063706
PE-conjugated mouse anti-rabbit IgG	Santa Cruz	Cat# sc-3753; RRID:AB_628498
FITC-conjugated anti-rat CD90/mouse CD90.1 (Thy-1.1) (clone OX-7)	BioLegend	Cat# 202504; RRID:AB_1595653
Chemicals, peptides, enzymes and recombinant proteins		
PE-conjugated Streptavidin	BioLegend	Cat# 405203
APC-conjugated Streptavidin (High Concentration)	BioLegend	Cat# 405243
7-AAD Viability Staining Solution	BioLegend	Cat# 420404
RBC Lysis Buffer (10X)	BioLegend	Cat# 420301
DAPI	Life Technologies	Cat# D3571
Human BD Fc Block	BD Pharmingen	Cat# 564220
Purified Rat Anti-Mouse CD16/CD32 (Mouse BD Fc Block)	BD Pharmingen	Cat# 553142
Phosphate-Buffered Saline, 1X without calcium and magnesium	Corning	Cat# 21-040-CV
Fetal Bovine Serum	Gibco	Cat# 10099141
RPMI 1640 Medium	Gibco	Cat# 11875119
DMEM, 1×	Corning	Cat# 10-013-CVRC
NK92 Medium	Cobioer	Cat# CBP60980M
GMP SCGM (Serum-free Stem Cell Growth Medium)	CellGenix	Cat# 20802-0500
Primary lung cancer medium	SUNNCELL	Cat# SNPM-H045
Primary colon cancer medium	SUNNCELL	Cat# SNPM-H136
Primary liver cancer medium	SUNNCELL	Cat# SNPM-H066
GlutaMAX™ Supplement	Gibco	Cat# 35050061
L-Glutamine 200mM(100×)	Gibco	Cat# 25030-081
Opti-MEM™ I Reduced Serum Medium	Gibco	Cat# 31985070
Penicillin-Streptomycin (5,000 U/mL)	Gibco	Cat# 15070063
Puromycin Dihydrochloride	Gibco	Cat# A1113803
Blasticidin S HCl (10 mg/mL)	Gibco	Cat# A1113903
Lipofectamine™ 2000 Transfection Reagent	Invitrogen	Cat# 11668019
Dimethyl sulfoxide	Sigma-Aldrich	Cat# D4540
TRIzol™ Reagent	Invitrogen	Cat# 15596018
MACS® Tissue Storage Solution	Mitenyi Biotec	Cat# 130-100-008
DEAE-Dextran hydrochloride	Sigma-Aldrich	Cat# D9885
Lymphoprep	STEMCELL Technologies	Cat# 07801
EDTA Unmasking Solution (10X)	Cell signaling technology	Cat# 14747S
Polybrene Infection/Transfection Reagent	Sigma-Aldrich	Cat# TR-1003-G
Ampicillin	Sigma-Aldrich	Cat# A5354

(*Continued on next page*)

Please cite this article in press as: Li et al., IGSF8 is an innate immune checkpoint and cancer immunotherapy target, Cell (2024), https://doi.org/10.1016/j.cell.2024.03.039

Continued

REAGENT or RESOURCE	SOURCE	IDENTIFIER
IL-2, Human	GenScript	Cat# Z00368
IL-15, Mouse	GenScript	Cat# XM_006530712.2
Poly(I:C) (LMW)	InvivoGen	Cat# tlrl-picw
TrypLE™ Select Enzyme (1X), no phenol red	Thermo Fisher Scientific	Cat# 12563011
Fixable Viability Dye eFluor™ 780	Thermo Fisher Scientific	Cat# 65-0865-14
CFSE	Thermo Fisher Scientific	Cat# 65-0850-84
CellTrace™ CFSE Cell Proliferation Kit, for flow cytometry	Thermo Fisher Scientific	Cat# C34554
DAPI	Thermo Fisher Scientific	Cat# 62248
EZ-Link® NHS-Biotin Reagents	Thermo Fisher Scientific	Cat# 20217
Dynabeads™ MyOne™ Streptavidin T1	Thermo Fisher Scientific	Cat# 65602
Collagenase, Type IV	Thermo Fisher Scientific	Cat# 17104019
DNase I	Roche	Cat# 10104159001
Novo-TSA	WiSee	Cat# H-D110051
SDS-PAGE Gel	GenScript	Cat# M42012
AR9 buffer, 10X	PerkinElmer	Cat# AR900250ML
Cas9-C-NLS Nuclease	GenScript	Cat# Z03385
NLS-Cas9-EGFP Nuclease	GenScript	Cat# Z03393
Protease and Proteinase K	QIAGEN	Cat# 19133
BsmbI	New England Biolabs	Cat# R0580
XbaI	New England Biolabs	Cat# R0145S
BamHI-HF	New England Biolabs	Cat# R3136S
T4 DNA Ligase	New England Biolabs	Cat# M0202S
T4 Polynucleotide Kinase	New England Biolabs	Cat# M0201S
High-Fidelity DNA Polymerase	New England Biolabs	Cat# M0491S
4% Paraformaldehyde Fix Solution	Sangon Biotech	Cat# E672002-0100
HEPES	Sangon Biotech	Cat# A100485
Sodium chloride	Sangon Biotech	Cat# A100241
EDTA	Sangon Biotech	Cat# A100105
Glycine	Sangon Biotech	Cat# A110167
Tween 20	Sangon Biotech	Cat# A600560
Recombinant protein A	Solarbio	Cat# P6860
Recombinant IGSF8-FC (LALAPG):	This paper	N/A
Recombinant IGSF8-His (8)	This paper	N/A
Recombinant KIR3DL2-FC	This paper	N/A
Recombinant KIR2DL1-FC	This paper	N/A
Recombinant KIR2DL2-FC	This paper	N/A
Recombinant KIR2DL3-FC	This paper	N/A
Recombinant KIR3DL1-FC	This paper	N/A
Recombinant KIR3DL3-FC	This paper	N/A
Recombinant Klra1-FC	This paper	N/A
Recombinant Klra2-FC	This paper	N/A
Recombinant Klra3-FC	This paper	N/A
Recombinant Klra5-FC	This paper	N/A
Recombinant Klra6-FC	This paper	N/A
Recombinant Klra9-FC	This paper	N/A
Recombinant Lacutamab-VH	This paper	N/A
Recombinant Lacutamab-VL	This paper	N/A

(*Continued on next page*)

Continued

REAGENT or RESOURCE	SOURCE	IDENTIFIER
Critical commercial assays		
MojoSort™ Mouse NK Cell Isolation Kit	BioLegend	Cat# 480050
NK Cell Isolation Kit, human	Miltenyi Biotec	Cat# 130-092-657
CD90.1 MicroBeads	Miltenyi Biotec	Cat# 130-121-273
Expi293™ Expression System Kit	Gibco	Cat# A14635
ExpiFectamine™ 293 Transfection Kit	Gibco	Cat# A14525
ExpiCHO™ Expression System Kit	Gibco	Cat# A29133
ExpiFectamine™ CHO Transfection Kit	Gibco	Cat# A29131
TruSeq RNA Library Prep Kit	Illumina	Cat# RS-122-2001; RS-122-2002
Amine Coupling Kit	Cytiva	Cat# BR100050
pcDNA™3.4 TOPO™ TA Cloning Kit	Thermo Fisher Scientific	Cat# A14697
Deposited data		
Public RNA-seq data	Riaz et al., 2017[48]	GEO: GSE91061
Public RNA-seq data	Hugo et al., 2016[56]	GEO: GSE78220
Public single-cell RNA-seq data	Pelka et al., 2021[47]	GEO: GSE178341
TISCH2 database	Han et al., 2023[46]	http://tisch.comp-genomics.org
RNA-seq data from cancer patients	Genomic Data Commons	https://portal.gdc.cancer.gov/
DNA copy number variation and mRNA alterations	cBioPortal	https://www.cbioportal.org/
Proteomics data for breast and ovarian tumors	Mertins et al., 2016,[54] Zhang et al., 2016[55]	N/A
HLA and KIR3DL2 allotypes of TCGA samples	Song et al., 2023[58]	N/A
RNA-seq data of syngeneic tumors treated with IGSF8.06 antibody and isotype controls	This study	ENA: PRJEB75001
RNA-seq data of B16-F10 Igsf8 KO and control tumors	This study	ENA: PRJEB75001
RNA-seq data of human and mouse NK cells that were highly and lowly bound to IGSF8 or Igsf8 proteins	This study	ENA: PRJEB75001
TCGA clinical data	Liu et al., 2018[74]	N/A
Experimental models: Organisms/strains		
C57BL/6	SMOC	Cat# SM-001
BALB/c	SMOC	Cat# SM-003
Experimental models: Cell lines		
Endura Competent Cells	Lucigen	Cat# 60242-1
NK92 cells	Cobioer	Cat# CBP60980
K562 bearing membrane-bound IL21	Yan et al., 2020[75]	N/A
Primary lung cancer cells	SUNNCELL	Cat# SNP-H045
Primary colon cancer cells	SUNNCELL	Cat# SNP-H136
Primary liver cancer cells	SUNNCELL	Cat# SNP-H066
293FT cells	Procell	Cat# CL-0313
PC9 cells	Procell	Cat# CL-0668
COLO205 cells	ATCC	Cat# CCL-222
AGS cells	ATCC	Cat# CRL-1739
K562 cells	ATCC	Cat# CCL-243
PC9 cells	ATCC	Cat# CRL-3228
A375 cells	ATCC	Cat# CRL-1619

(*Continued on next page*)

Please cite this article in press as: Li et al., IGSF8 is an innate immune checkpoint and cancer immunotherapy target, Cell (2024), https://doi.org/10.1016/j.cell.2024.03.039

Continued

REAGENT or RESOURCE	SOURCE	IDENTIFIER
NCI-H520 cells	ATCC	Cat# HTB-182
B16-F10 cells	ATCC	Cat# CRL-6475
LLC (LL/2 (LLC1)) cells	ATCC	Cat# CRL-1642
CT26 cells	ATCC	Cat# CRL-2638
EMT6 cells	ATCC	Cat# CRL-2755
Oligonucleotides		
gAAVS1: GCTCATCCAGAGACGGGGAT	This paper	N/A
gRosa26: ACTCCAGTCTTTCTAGAAGA	This paper	N/A
human *IGSF8* gRNA1: GAGGGGCCCTTGTACCGCG	This paper	N/A
human *IGSF8* gRNA2: GGTACCGCATGGTAGTAGG	This paper	N/A
mouse *Igsf8* gRNA1: CACGCCTCACAGTGCACGA	This paper	N/A
mouse *Igsf8* gRNA2: GCAGTTCTAAGGGTTCGCCT	This paper	N/A
Recombinant DNA		
lentiCRISPR v2	Addgene	Cat# 52961
lentiGuide-Puro	Addgene	Cat# 52963
lentiCas9-Blast	Addgene	Cat# 52962
pMD2.G	Addgene	Cat# 12259
psPAX2	Addgene	Cat# 12260
pcDNA™3.1/His A, B, & C Mammalian Expression Vectors	Thermo Fisher Scientific	Cat# V38520
Software and algorithms		
Kaluza Analysis Software	Beckman Coulter	RRID:SCR_016182
FlowJo Software Version 10.8.1	FlowJo, LLC	RRID:SCR_008520
MAGeCK Version 0.5.8	Li et al., 2014[14]	https://bitbucket.org/liulab/mageck/
Bioinformatics analyses	This paper	https://github.com/gv20-therapeutics/IGSF8-NK
Scanpy Version 1.9.3	Wolf et al., 2018[76]	https://scanpy.readthedocs.io/
AlphaFold2	Jumper et al., 2021[77]	https://alphafold.ebi.ac.uk/
US-align	Zhang et al., 2022[78]	https://zhanggroup.org/US-align/
GraphPad Prism Version 9	Prism	RRID: SCR_002798

RESOURCE AVAILABILITY

Lead contact

Further information and requests for resources and reagents should be directed to and will be fulfilled by the lead contact, Tengfei Xiao (tengfei_xiao@gv20tx.com).

Materials availability

Correspondence and requests for materials should be addressed to the lead contact. The unique identifiers of all biological materials are listed in the key resources table. The newly generated recombinant proteins can be obtained from the lead contact following reasonable requests.

Data and code availability

- The RNAseq data of patients with solid tumors were obtained from the Genomic Data Commons (GDC) data portal (https://portal.gdc.cancer.gov/) on 13.11.2022. DNA copy number variation and mRNA alterations were downloaded from cBioPortal (https://www.cbioportal.org/) for the estimation of IGSF8 alterations. The mass spectrometry-based proteomics data for breast and ovarian tumors were retrieved from the CPTAC projects.[54,55] The TCGA clinical data used in this study were sourced from the publication by Liu et al.[74] The HLA and KIR3DL2 allotypes of TCGA samples were determined using T1K.[58] To investigate the

expression of IGSF8 in responders and non-responders upon anti-PD1 treatment, we accessed publicly available RNA-seq data from two clinical studies, accessible at GEO under accession number GSE9106156 and GSE7822055. The accession numbers for all these existing, publicly available datasets are also listed in the key resources table. The processed CRISPR screen data reported in this paper is included in the supplementary information files. Raw RNA-seq data have been deposited at ENA under assession number PRJEB75001. Microscopy data reported in this paper will be shared by the lead contact upon request.

- All codes for data analysis and visualization have been deposited at https://github.com/gv20-therapeutics/IGSF8-NK and are publicly available as of the date of publication.
- Any additional information necessary to re-analyze the data reported in this paper is available from the lead contact upon request.

EXPERIMENTAL MODEL AND STUDY PARTICIPANT DETAILS

Cancer cell culture

The COLO205, AGS, 293FT, K562, PC9, A375, NCI-H520, B16-F10, LLC, CT26 and EMT6 were obtained from ATCC and Procell, and the cells were cultured in RPMI 1640, with 10% heat-inactivated FBS and penicillin/streptomycin (100U/ml), L-glutamine (2mM) and incubated at 37°C with 5% CO_2. All cell lines were confirmed to be mycoplasma free by PCR. The NK92 cell line was obtained from Cobioer (CBP60980) and was cultured in the NK92 medium provided by Cobioer (CBP60980M). Primary lung cancer, colorectal cancer, and liver cancer malignant cells, as well as the related culture medium, were purchased from commercial vendor SUNNCELL (https://www.sunncell.com.cn/ydxb). The cells were cultured according to the manufacturer's instructions.

Primary NK culture

To conduct co-culture experiments, primary NK cells were isolated from multiple anonymous healthy donors. $CD56^+$ NK cells were isolated using an NK cell negative selection kit (Miltenyi) and subsequently cultured in SCGM media (CellGenix) supplemented with 10% heat-inactivated FBS, 200U/ml IL-2 (Genscript), penicillin/streptomycin (100U/ml), L-glutamine (2mM). The cells were cultured at a target density of $0.5*10^6$ cells/mL.

Primary NK cell expansion

Peripheral blood mononuclear cells (PBMCs) were isolated from healthy donors using Lymphoprep (Stem Cell). For expanding human NK cells, 20 million PBMCs were cultured with 20 million 10,000-rad-irradiated feeder cells (K562 bearing membrane-bound IL21 (K562-mbIL21[75]) in 30 mL RPMI 1640 media containing 10% FBS (Gibco), 2 mM L-glutamine (Gibco), 100 U/ml penicillin-streptomycin (Gibco), 200 U/ml IL-2 (Genscript) in cell culture plates (Corning) at a target density of 1×10^6/mL. The media were changed every 3–4 days and re-stimulated with the K562-mbIL21 after seven days. The total cell numbers were counted using the automated cell counter (Countstar) with trypan blue. To determine the percentage of NK cells, the cells were stained for CD3 and CD56 and analyzed by flow cytometry. Primary mouse NK cells were isolated from female C57BL/6 splenocytes using a negative isolation kit (BioLegend), according to the manufacturer's instructions. NK cells were cultured in RPMI 1640 medium supplemented with 10% FBS, penicillin/streptomycin (100U/ml), L-glutamine (2mM), non-essential amino acids (0.1mM), sodium pyruvate (1mM), HEPES (25mM), 2-ME (0.05mM) and recombinant mouse IL-15 (10 ng/ml; Genscript) and incubated at 37°C with 5% CO_2. Primary effector cells were used after 6 or 7 days of culture.

Syngeneic tumor studies

The B16-F10, LLC, CT26 and EMT6 cells were cultured as described above. Six-week-old female C57BL/6, BALB/c were subcutaneously inoculated with 0.5×10^6 of B16-F10, LLC, CT26 and EMT6 cells per mouse. Tumor growth was monitored by a caliper. When tumors reached an average volume of ~100 mm^3, typically 5–7 days after implantation, mice were randomized into groups based on tumor volume (n = 7 or 8 mice per group). The mice were then treated with the isotype-matched IgG controls, IGSF8.06, anti-PD1 (clone 29F.1A12, BE0273, Bioxcell), anti-CD4 (BE0119, Bioxcell), anti-CD8b (BE0223, Bioxcell) or anti-NK1.1 (BE0036, Bioxcell) antibodies at different doses, and administered three or four times by intraperitoneal injection every 3 days. All mouse experiments were carried out at the Shanghai Model Organisms Center with ISO 9001 certificate. Researchers in the center were blinded to treatment assignments. Animals were continuously monitored, and mice were euthanized via asphyxiation when any of the following endpoints were met: study termination, tumor burden equal or greater than 3000 mm^3, tumor ulceration, body weight loss equal or greater than 20%, or moribund appearance. Mice whose tumors were unmeasurable or below 20 mm^3 were considered to be tumor-free.

METHOD DETAILS

CRISPR screens

CRISPR screens in cancer cell lines

Genome-wide CRISPR screens were used to identify determinants of COLO205 or AGS cell response versus resistance to NK cells. The genome-wide gRNA library comprising 104780 gRNAs targeting 18749 genes (Table S1), and the cell surface gRNA library

Please cite this article in press as: Li et al., IGSF8 is an innate immune checkpoint and cancer immunotherapy target, Cell (2024), https://doi.org/10.1016/j.cell.2024.03.039

comprising 12000 gRNAs targeting 2797 genes (Table S2) were designed using published algorithm.[79] The gRNA oligos were synthesized at Twist Bioscience. After PCR amplification of the oligos and ligated into the lentiCRISPR v2 vector[80] using the Gibson Assembly Cloning system (NEB), followed by transforming the construct into competent cells for expansion. The oligo representation and coverage were tested before screening by deep sequencing. The lentiviral CRISPR library was delivered to COLO205 or AGS cells at a low multiplicity of infection (MOI) (0.3–0.5) with 200–500 cells per gRNA coverage, to ensure that most cells receive only 1 viral construct with high probability as described previously.[81] After puromycin selection (2 μg/mL) for 5 days, the surviving cells were divided into three groups (one was control, and the others were co-cultured with the expanded NK cells from two or three different donors as biological replicates overnight). The selected E:T ratio was selected to kill ~50% of the malignant cells. The NK cells and dead COLO205 or AGS cells were further removed by discarding the culture medium and washed with cold PBS buffer (4°C) twice before genomic DNA extraction. Two rounds of PCR were performed after gDNA had been extracted as described previously,[81] each library was sequenced at 30–40 million reads to achieve ~300X average coverage over the CRISPR library.

CRISPR screens in expanded NK cells

A focused gRNA library targeting 2797 cell surface genes was used to identify the interaction partner of IGSF8 on the human NK cells. The lentiviral gRNA library was synthesized, amplified, and ligated into the homemade lentiGuide-thy1.1 vector by substituting the thy1.1 gene for puroR of lentiGuide-puro vector (Addgene). The screens in primary NK cells were further carried out combining pooled lentiviral gRNA delivery with Cas9 protein electroporation. On day 1, the viral supernatant for a MOI between 30 and 50 of the titered virus with 4 μg/mL dextran sulfate (D9885-10G, Sigma) were added to 100 million expanded NK cells with culture medium at a target density of 1×10^6/mL. The spinfection of these NK cells was carried out using four of 12-well plates with 2×10^6 cells per well and centrifuged at 2000g for 90 min at room temperature. After removing the medium, the NK cells were resuspended with fresh culture medium and pooled together into larger flasks. The following morning, the spinfection of these NK cells was repeated using the same method. On day 4, the Thy1.1+ NK cells were sorted by MACS using anti-CD90.1 microbeads (Miltenyi). On day 5, the Thy1.1+ NK cells were collected, and resuspended in Lonza electroporation buffer P3 at 2×10^7 cells in 100μL. Next, 20μL NLS-Cas9-EGFP protein (Genscript, 16 μM stock) was added to the cell suspension. Cells were electroporated at 20 million cells per cuvette using the EN-138 program. Immediately after electroporation, 1mL of pre-warmed media was added to each cuvette and cuvettes were placed at 37°Cfor 20 min. The cells were then transferred to the NK culture medium. After electroporation, the expression of EGFP was detected in NK cells to ensure that more than 70% of the NK cells showed detectable EGFP signal. On day 7, the Thy1.1+ NK cells by MACS using CD90.1 microbeads (Miltenyi), followed by expanding the NK cells in NK culture medium for seven more days. On day 14, the NK cells were ready for cell surface staining of IGSF8 receptors. For cell surface staining of IGSF8 receptor using biotinylated IGSF8-his protein on NK cells, the edited NK cells were co-cultured with K562 cells overnight. Next day, samples were harvested and stained in the fixable viability dye eFluor780 and surface staining with the anti-human CD56 antibody, biotinylated IGSF8-his protein, Fc blocker, and streptavidin-PE on ice for 30 min before sorting by flow cytometry. The 10^{th} percentile of NK cells with high or low IGSF8 protein binding signal were further collected before genomic DNA extraction and gRNA library preparation for high-throughput sequencing as described previously.[81]

Deorphaning the IGSF8 receptor on NK cells by differential RNA-seq

To perform the sorting experiments, 2×10^7 human expanded NK cells were incubated with fixable viability dye eFluor780, anti-human CD56 antibody, biotinylated IGSF8-his protein (20 μg/mL), Fc blocker, and streptavidin-PE on ice for 30 min. The cells were then sorted based on their binding to IGSF8 protein, with cells below the 10th and above the 90th percentile of binding selected.

For the mouse splenic NK cell sorting experiment, C57BL6 mice were intravenously injected with Poly (I:C) (LWM, 300 μg/mouse in PBS), and 16 h later, their spleens were harvested. The spleen was placed on a cell strainer and treated with RBC lysis buffer (BioLegend) to remove red blood cells. The splenic NK cells were isolated using a negative isolation kit (BioLegend), according to the manufacturer's instructions. Then, anti-CD45, -CD19, -CD3, -NK1.1 antibodies, viability dye, biotinylated mouse Igsf8-his protein (20 μg/mL), Fc blocker, and streptavidin-PE were added to the cells on ice and incubated for 30 min. The splenic NK cells were sorted by flow cytometry, selecting the cells that were $CD45^+CD19^-CD3^-NK1.1^+$ and with binding to Igsf8 protein below the 10th and above the 90th percentile. RNA extraction was performed using trizol (Invitrogen) on the two sorted groups of NK cells, followed by library construction using the TruSeq RNA Library Prep Kit (Illumina) for Illumina Hi-Seq.

Cell binding and blocking assays

CT26 cells transduced with KIRs, IGSF8 (human, cynomolgus monkey, or mouse) expression, were generated by lentiviral particles. The cDNAs of KIR family genes and IGSF8 were synthesized by Genewiz. These cDNA were then cloned into the lentiCas9-blast (Addgene) lentiviral vector by replacing its Cas9 gene. Overexpression of KIR and *IGSF8* genes in cells was confirmed by detecting their corresponding antibodies and verifying that the target genes had over 90% expression relative to control cells. To test IGSF8-Fc/his protein binding to the CT26 cells, NK, or T cells, the biotinylated IGSF8 protein (20 μg/mL) was used. For cell surface staining, 100,000 cells overexpressing the antigen were washed with a PBS buffer containing 2% FBS, and then incubated with IGSF8.06 antibody or IgG isotype of different concentrations for 30 min on ice. Cells were then washed with PBS containing 2% FBS and incubated with 1:100 anti-human Fc-PE antibody for 15 min on ice. Cells were washed and analyzed on a flow cytometric analyzer (CytoFlex, Beckman). The MFI was plotted vs. antibody concentration. The EC50 cell binding potency was calculated using nonlinear regression curve fit. For IGSF8 antibody blocking assays, the CT26 cells expressing human or mouse IGSF8 were pre-incubated with

IGSF8.06 antibody or IgG isotype control at different concentrations plus 20 μg/mL biotinylated KIR3DL2-hFc or Klra9-hFc proteins. The binding signals were detected by streptavidin-PE. For anti-KIR3DL2 antibody blocking assays, the expanded NK cells were pre-incubated with anti-KIR3DL2 (R&D) at different concentrations plus 20 μg/mL biotinylated IGSF8-his proteins.

Ex vivo mouse leukocyte profiling

B16-F10 tumors were enzymatically disassociated with 300U/ml collagenase IV (Thermo Fisher Scientific) and 100 μg/mL DNase I (Roche) in HBSS supplemented with 5% v/v heat-inactivated FBS and 5 mM $CaCl_2$ and mechanically disassociated with GentleMacs cell disruptors (Miltenyi). Then cells were stained with the antibodies against CD45, CD3, CD4, CD8, CD11b, CD11c, F4/80, and NK1.1, as well as cell viability dye. The $CD4^+$ T cells ($CD3^+CD4^+$), $CD8^+$ T cells ($CD3^+CD8^+$), NK cells ($CD3^-$, $NK1.1^+$), macrophages ($CD11b^+$, $F4/80^+$), and DCs ($CD11c^+$ $F4/80^-$) were analyzed by flow cytometry. Fc receptor blocking was performed with anti-CD16/CD32 (2.4G2, BD Biosciences).

Lentivirus production and purification

T-225 flasks of 293FT cells were cultured at 40%–50% confluence the day before transfection. Transfection was performed using Lipofectamine 2000 (Life Technologies). For each flask, 20 μg of lentivectors, 5 μg of pMD2.G, and 15 μg of psPAX2 (Addgene) were added into 4 mL OptiMEM (Life Technologies). 100 μL of Lipofectamine 2000 was diluted in 4 mL OptiMEM and, after 5 min, it was added to the plasmid mixture. The complete mixture was incubated for 20 min before being added to cells. After 6 h, the media was changed to 30 mL DMEM +10% FBS. After 60 h, the media was removed and centrifuged at 500 g at 4°C for 10 min to pellet cell debris. The supernatant was filtered through a 0.45 μm low protein binding membrane. The virus was subjected to ultracentrifugation at 20,000 g for 2 h at 4°C, followed by overnight resuspension at 4°C in DMEM +10% FBS. Aliquots were then stored at −80°C.

Gene essentiality in cell lines

To know the gene essentiality of *IGSF8*, we downloaded cell growth CRISPR screen data for 1,054 cell lines from DepMap (https://depmap.org/portal/download/). We defined the overall essentiality as an average of all dependency scores in the data because more negative dependency scores mean more essential to cell growth. We showed the overall essentiality scores for *IGSF8* and other known cell-essential genes such as TP53, CDK1, CDK2, and MYC. Further, we downloaded matched RNA-seq expression data from DepMap to evaluate the correlation between dependency scores and gene expression levels. Expression values in Transcripts Per Million reads (TPM) were log2 transformed with pseudocount 1 added. The correlation coefficients and *p*-values were measured by Spearman's rank correlation.

Human and mouse NK cytotoxicity assay

Carboxyfluorescein succinimidyl ester (CFSE, ThermoFisher Scientific) labeling of malignant cells combined with 7-AAD solution (BioLegend) staining of dead cells is a reliable method to measure *in vitro* cell killing by flow cytometry. Briefly, target malignant cells were labeled with CFSE (C34554, Invitrogen) for 15 min at 37°C in RPMI-1640 medium with 1% FBS, protected from light, washed twice with RPMI-1640 with 2% FBS and resuspended in RPMI-1640 with 10% FBS to quench the labeling reaction. Adherent malignant cells were cultured one night before co-culture with effector NK cells. Suspended malignant cells were immediately co-cultured with different ratios of NK cells as previously described.[82] Briefly, 2×10^4 CFSE-positive K562 cells were co-cultured with various effector: target (E: T) ratios as indicated for 4 h (co-culture of adherent malignant cells could be extended up to overnight) at 37°C in a humidified 5% CO_2 incubator. Then, samples were harvested and stained in 7-AAD solution (BioLegend) on ice for 20 min before cytometry analysis (CytoFlex S, Beckman). The NK cell-mediated cytotoxicity was calculated by the percentage of 7-AAD-positive malignant cells among total malignant cells. Spontaneous cancer cell death, in the absence of NK, was less than 5%, and subtracted from total killing in the presence of NK cells or PBMCs. All flow cytometry data were analyzed by Kaluza or FlowJo (v10.8.1) software.

Multiplexed immunohistochemistry staining

Human cancer tissue microarrays (TMAs) were acquired from (US Biomax). Antigen retrieval was carried out by subjecting the TMAs to Leica Bond ER2 at 100°C for 20 min. The formalin-fixed paraffin-embedded slides were blocked with a 3% hydrogen peroxide solution at room temperature (RT) for 10 min, and then with 5% normal goat serum at RT for 1 h. The primary antibodies employed in this study were anti-IGSF8 (HPA011917, Sigma), anti-HLA-A/B (ab134189, Abcam, may cross-react with HLA-C and HLA-E based on manufacturer's instructions), and anti-pan cytokeratin (GM351507, Gene Tech), utilized according to the manufacturer's instructions, and incubated for 60 min at RT. Subsequently, goat anti-mouse Poly HRP secondary antibody or goat anti-rabbit Poly HRP secondary antibody (Thermo Fisher Scientific, B40961 and B40962) were applied at RT for 10 min. The HRP-conjugated secondary antibody polymer was then detected using Novo-light TSA 570, 620, and 670 (WiSee) to amplify the fluorescent tyramide signal. Following the covalent tyramide reaction, heat-induced stripping of the primary antibody-secondary antibody complex was performed using PerkinElmer AR9 buffer (AR900250ML) and Leica Bond ER2 (90% ER2 and 10% AR9) at 100°C for 20 min before proceeding to the next staining cycle. After three sequential rounds of staining, the slides were mounted using Gold Antifade Mountant with DAPI (Thermo Fisher Scientific). Each staining included positive and negative controls (FFPE cell blocks).

Please cite this article in press as: Li et al., IGSF8 is an innate immune checkpoint and cancer immunotherapy target, Cell (2024), https://doi.org/10.1016/j.cell.2024.03.039

Surface plasmon resonance

The BIAcore utilizes the optical properties of surface plasmon resonance (SPR) to detect alteration in protein concentration of interacting molecules within a dextran biosensor matrix. CMD500M chips (SCBS CMD500M) were purchased from Xantec. HEPES (A100485), NaCl (A100241), EDTA (A100105) and Glycine (A110167) were purchased from Sangon. All measurements were performed at 25°C. Samples were dissolved in HBS-EP+ buffer (150 mM NaCl, 3 mM EDTA, 0.05% w/v Tween 20, and 10 mM HEPES, pH 7.4). Recombinant protein A (P6860, Solarbio) was immobilized on the sensor chip at a level of 9000-1000 response unit (RU) using an amine coupling kit (BR100050, Cytiva). Binding was evaluated using multi-cycle kinetics. Each cycle was performed at a flow rate of 30 μL/min and consisted of the following steps: injection of antibodies to the finial RU about 900 RU, injection of IGSF8.06 or KIR3DL2-Fc for 120 s (0 μg/mL for blank and 0.5 μg/mL for test) followed by a dissociation stage for 300 s or 450 s, and regeneration using 30 s injection of 10 mM Gly-HCl, pH 1.5. Association and dissociation rates for each cycle was determined by fitting the sensorgram data using to a 1:1 binding model to calculate the Ka, and Kd; the equilibrium binding constant KD was calculated using the relationship KD = Kd/Ka.

Antibody discovery for IGSF8

Monoclonal antibodies against IGSF8 were generated *in silico* using a proprietary computer-assisted design algorithm, which generates sequences of fully human monoclonal antibodies against different targets, partly by taking advantage of the available sequences from human BCR (B cell receptor) repertoires. This technology enables speedy design of numerous monoclonal antibodies against given targets. For example, more than a hundred monoclonal antibodies against human IGSF8 were discovered by this method. After the heavy chain and light chain sequences of these antibodies were obtained, monoclonal antibodies were cloned to pcDNA3.4 vector and expressed by ExpiCHO cells (Thermo Fisher Scientific). The antibodies were further screened for high affinity binders to full-length IGSF8 using surface plasmon resonance (SPR) by BIAcore T100. IGSF8.06 was chosen to be the lead antibody.

Gene knockout by CRISPR

The lentiviral gIGSF8 vectors were generated by ligation of hybridized oligos (gRNAs) into lentiCRISPR-V2 vectors (Addgene) linearized with BsmBI using quick ligase (NEB). Malignant cells were transduced with viral particles mixed with polybrene (8 μg/mL) and selected by puromycin for three days. The IGSF8 knockout efficiency in different malignant cells was tested by anti-IGSF8 antibody (Sino) using flow cytometry.

Gene overexpression by lentiviral particles

Genewiz synthesized the cDNAs of HLA-C, IGSF8, KIRs, or HA-tag. These cDNA were then cloned into the lentiCas9-blast (Addgene) lentiviral vector by replacing the Cas9 gene. After packaging lentiviral particles, malignant cells (K562, NK92 or CT26) were transduced with the viral particles mixed with polybrene (8 μg/mL) by spinfection, as described above. The cells were then selected by blasticidin for 3 days.

Recombinant protein and antibody expression and quality control

Recombinant proteins were produced in Expi293 cells (Thermo Fisher Scientific) by transiently transfection with pcDNA3.4 plasmids (Thermo Fisher Scientific) containing the cDNA of interest. The transfected cells were cultured in Expi293 Expression medium (Thermo Fisher Scientific) for 5 days before collecting the conditioned supernatant. The recombinant proteins were then purified using Ni^{2+} or protein A affinity chromatography, followed by size exclusion chromatography (SEC, Superdex200) through AKTA Explorer. The quality of the purified proteins and the formation of disulfide-linked complexes were confirmed by SDS-PAGE and HPLC-SEC. Antibodies were expressed by co-transfecting Expi293 cells with pcDNA3.4 plasmids encoding the heavy and light chains of interest. Human IgG1 and mouse IgG2a antibodies were purified using protein A capture followed by SEC. The extracellular domains of human IGSF8, KIR, and Klra family genes were synthesized and cloned into the pcDNA3.4 vector, with an Fc tag. The Fc tag sequence used included L234A L235A P329G mutations, which do not bind to Fc receptors.[83] In line with previous studies that have shown the complex formed by the IGSF8 protein and CD9 is a dimeric structure,[84] we incorporated a human Fc hinge sequence between the extracellular domain and C-terminal 8x his tag of human or mouse IGSF8 protein to maintain this structure. The resulting fusion protein, with the sequence "DKTHTCPPCHHHHHHHH", facilitates the formation of a dimeric structure similar to IGSF8-Fc for the IGSF8-his protein. These constructs were then transiently transfected into Expi293 cells for protein expression by ExpiFectamine 293 Transfection Kit (Thermo Fisher Scientific). The biotin-labeled proteins were generated by EZ-Link NHS-Biotin (Thermo Fisher Scientific). The expression of the IGSF8.06 antibody involved cloning the heavy and light chain sequences into the pcDNA3.4 vector separately. The constructs were then transiently transfected into ExpiCHO cells using the ExpiFectamine CHO Transfection Kit for antibody expression, following the kit's instructions. Two versions of IGSF8.06 Fc were selected for expression, namely human IgG1 with L234A L235A mutations and mouse IgG2a with LALA mutations. For quality control by SDS-PAGE, 5 μg of samples were loaded onto a 4–20% SDS-PAGE gel (Genscript) and run under both reducing and non-reducing conditions.

QUANTIFICATION AND STATISTICAL ANALYSIS

CRISPR screening data analyzed by the MAGeCK algorithm

Sequencing data from CRISPR screens were processed and analyzed according to the MAGeCK workflow.[14,81] Briefly, raw sequencing reads were mapped to the sgRNA library using the MAGeCK *count* function that produces a sgRNA-by-sample read count matrix and a summary table for data quality. Next, the MAGeCK RRA algorithm (*mageck test* function) was used to select significantly enriched and depleted genes and sgRNAs in two comparable conditions. Control sgRNAs were used to normalize the data during the comparisons. Significant genes were visualized by custom R scripts. KEGG pathways were enriched by the R clusterProfiler package using a list of significant genes (p-value <0.01) identified in each screen.

Statistics and survival analysis

To ensure robust statistical analysis, a sample size filter was applied to exclude groups with fewer than 100 tumor samples or 10 normal samples. Differential expression analysis of IGSF8 was performed using Student's t-test. Spearman correlation was performed to evaluate the correlation between IGSF8 and selected immune-related markers. To investigate the occurrence of IGSF8 and B2M mRNA alterations in various tumor types, mRNA z-scores relative to tumor-adjacent normal tissues were acquired from cBioPortal. Tumor samples with z-scores greater than 1 were categorized as up-regulated, while those with z-scores less than −1 were considered down-regulated. This means that the expression levels of up-regulated tumor samples surpass approximately 84.1% of normal samples, while the expression levels of down-regulated tumor samples fall below 84.1% of normal samples. To assess the impact of IGSF8 expression on clinical outcomes, Cox proportional hazards regression models were employed. Initially, an MHCI score, defined as the average expression of HLA-A, HLA-B, HLA-C, B2M, TAP1, and TAP2, was calculated per patient. Then, patients within each cohort were grouped as MHCI high or MHCI low based on whether their MHCI scores were above or below average, respectively. Subsequently, the top and bottom 25% of patients with high and low IGSF8 expression, respectively, were compared while regressing out the effects of covariates such as age, cancer stage (early and late), and gender. It is worth noting that for the analysis of SKCM patients, we made a distinction between metastatic cases and primary tumors due to differences in initial diagnostic times between these groups – the initial diagnostic times for metastatic cases are the initial diagnostic times of non-metastatic diseases as reported previously.[74] Throughout the analysis, nominal p-values were reported given the limited number of hypothesis tests performed.

Analysis of public scRNA-seq datasets

The TISCH2 scRNA-seq data were downloaded from the TISCH2 Website.[46] To minimize batch effects, only scRNA-seq datasets generated on the 10x genomics platform were included. Further filtering was applied to exclude patients receiving any treatments, including targeted therapy, immunotherapy and/or chemotherapy. This resulted in approximately 4 million non-treated human cells across 46 diseases from 96 studies. The cells were subsequently renormalized by total counts over all genes to obtain UMI count per million (CPM) and followed by a log2 transformation. To examine the expression patterns at the single-cell level, both the average expression level and expression fraction of IGSF8 and KIR3DL2 per sample was calculated. The scRNA-seq data related to colorectal tumors, including expression metrics, cell annotations and metadata, were retrieved from GEO under GSE178341.[47] The analysis of scRNA-seq datasets was conducted using Scanpy.[47,76] In summary, each cell was normalized by total counts using the 'pp.normalize_total' with the parameter 'target_sum = $1e^6$' and a log transformation was performed using the 'pp.log1p' function. Subsequently, we computed the average expression level and expression fraction for IGSF8, KIR3DL2 and B2M per sample. For visualization of the three genes in a single plot (Figure 3D), we calculated the mean of the average expression levels and fractions across samples, normalizing the mean expression levels between 0 and 1 using the following equation:

$$normalized\ expression = \frac{log(CPM+1) - min\,(log(CPM+1))}{max(log(CPM+1)) - min(log(CPM+1))}$$

Structural similarities between MHC-I and IGSF8

The 3D structures of MHC class I and B2M proteins were extracted from 1P4L (PDB ID) for mice and 3VH8 (PDB ID) for humans. For 1P4L, based on sequence numbering in PDB database, MHC Class I H-2KB heavy chain was annotated as alpha1 (chainA:1–88), alpha2 (chainA:89–182) and alpha3 (chainA: 183–274), while the beta-2 microglobulin was chain B:1–99. Same processing method was applied to 3VH8, with HLA class I histocompatibility antigen B-57 was annotated as alpha1 (chainA:1–88), alpha2 (chainA:89–182) and alpha3 (chainA: 183–275), while the beta-2 microglobulin was chain B:1–99. The IGSF8 protein structure was predicted using Alphafold2,[77] with the Q969P0 (UniProt ID) sequence. The IGSF8 protein consists of four immunoglobulin domains: D1 (28–149), D2 (151–300), D3 (303–434) and D4 (437–573), and the entire extracellular domain (ECD, 28–573) was also considered in the similarity computation. US-align[78] was used to measure the structural similarity between the domains in the MHC-I complex and the domains in IGSF8. Two structures fold similarly when the measured TM-score is above 0.5.

CellPress

Supplemental figures

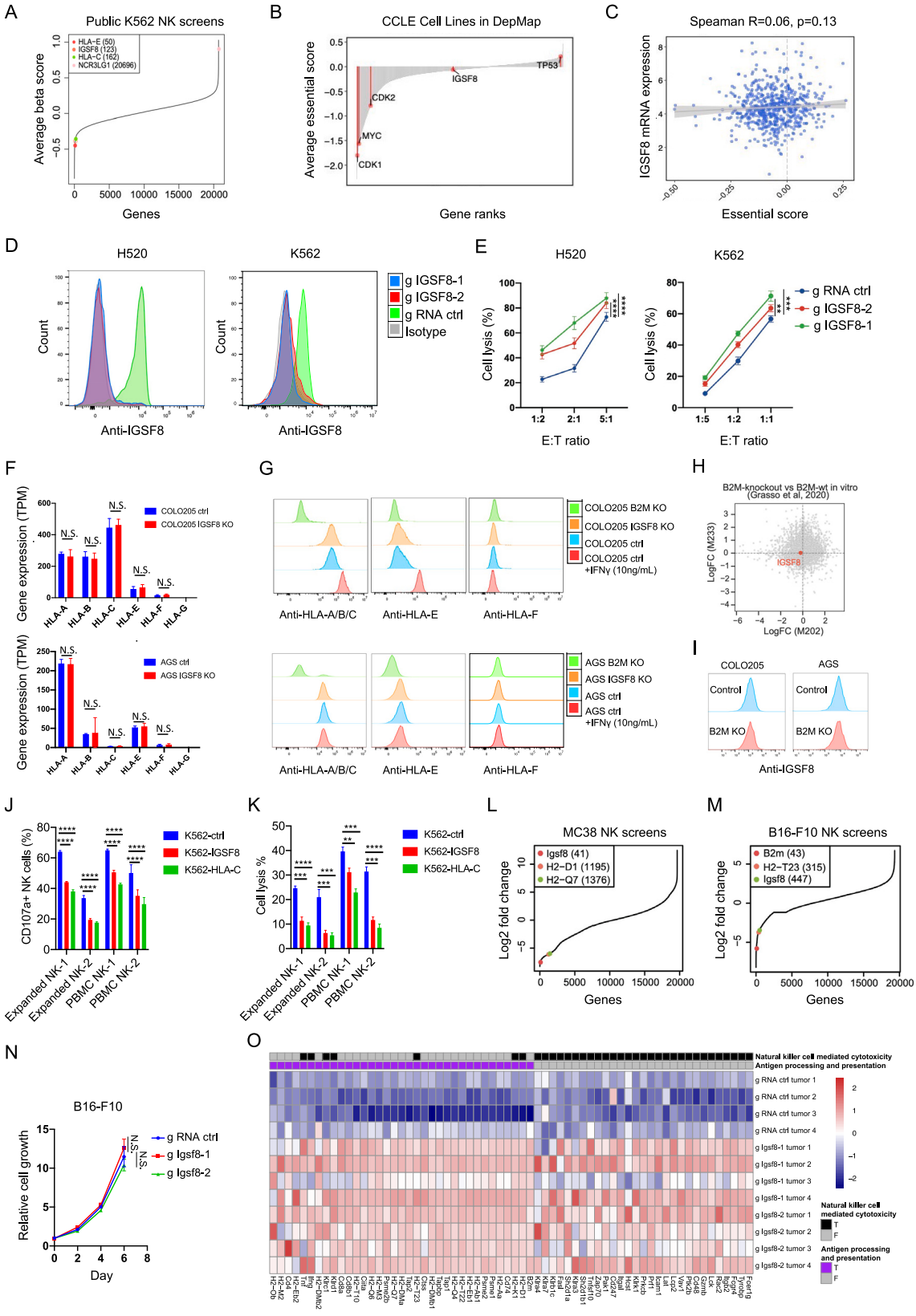

(legend on next page)

Figure S1. Identification of IGSF8 as a suppressor of NK cell function, related to Figure 1

(A) A published study[25] conducted a CRISPR screen on K562 cells and primary NK cell co-culture. IGSF8 and other known positive control genes are highlighted.

(B) Waterfall plot showing average essential scores of genes in CCLE cell lines from DepMap. IGSF8 and several known pan-essential genes were highlighted.

(C) Dot plot depicting IGSF8 gene expression and its essential scores in cancer cell lines. Data for gene expression and genetic dependency were obtained from the DepMap portal (deomap.org).

(D) Reduction in cell surface IGSF8 upon CRISPR/Cas9-mediated knockout of IGSF8 in H520 and K562 cells.

(E) NK cell-mediated cytotoxicity against H520 and K562 cells after CRISPR/Cas9-mediated knockout of IGSF8. Cytotoxicity was assessed through flow cytometric staining of the 7-AAD death marker. The E:T ratio represents the ratio of NK cells to H520 and K562 cells. The data are presented as mean ± SD ($n = 3$; a two-way ANOVA test, $^{**}p < 0.01$, $^{***}p < 0.001$, $^{****}p < 0.0001$).

(F) RNA expression of HLA genes in COLO205, AGS control and IGSF8-null cells. The transcripts per million (TPM) were calculated as described (Methods).

(G) Flow cytometry staining for HLA genes on COLO205 and AGS cells following CRISPR/Cas9-mediated knockout of IGSF8, B2M or AAVS1 (control).

(H) IGSF8 expression unchanged upon B2M knockout in two melanoma cell lines grown *in vitro*. Data from Grasso et al., 2020.[85].

(I) Flow cytometry staining for IGSF8 on COLO205 and AGS cells following CRISPR/Cas9-mediated knockout of B2M or AAVS1 (control).

(J) NK cell activation (as measured by CD107a) upon co-culturing with K562 cells overexpressing IGSF8, HLA-C, or HA-tag control for 4 h. NK cells used are either expanded NK cells, or purified PBMC NK cells from two healthy donors. The data are represented as mean ± SD ($n = 3$; two-tailed Student's t test, $^{***}p < 0.001$, $^{****}p < 0.0001$).

(K) NK cell-mediated cytotoxicity upon co-culturing with K562 cells overexpressing IGSF8, HLA-C, or HA-tag control for 4 h. The cytotoxicity was measured by flow cytometric staining of the death marker in the K562 cells. The data are represented as mean ± SD ($n = 3$; two-tailed Student's t test, $^{**}p < 0.01$, $^{***}p < 0.001$, $^{****}p < 0.0001$).

(L and M) Published studies[34,36] conducted CRISPR screens on MC38 cells (L) and B16-F10 cells (M) co-cultured with primary mouse NK cells. IGSF8 and other known positive control genes are highlighted.

(N) Cell growth of B16-F10 cells with either mouse gRNA ctrl (gRosa26) or mouse gIgsf8 was monitored over six days using an automated cell counter.

(O) Heatmap of differentially expressed genes in B16-F10 ctrl versus Igsf8-null tumors. The genes shown are from the top two enriched gene pathways (Natural killer cell-mediated cytotoxicity or Antigen processing and presentation).

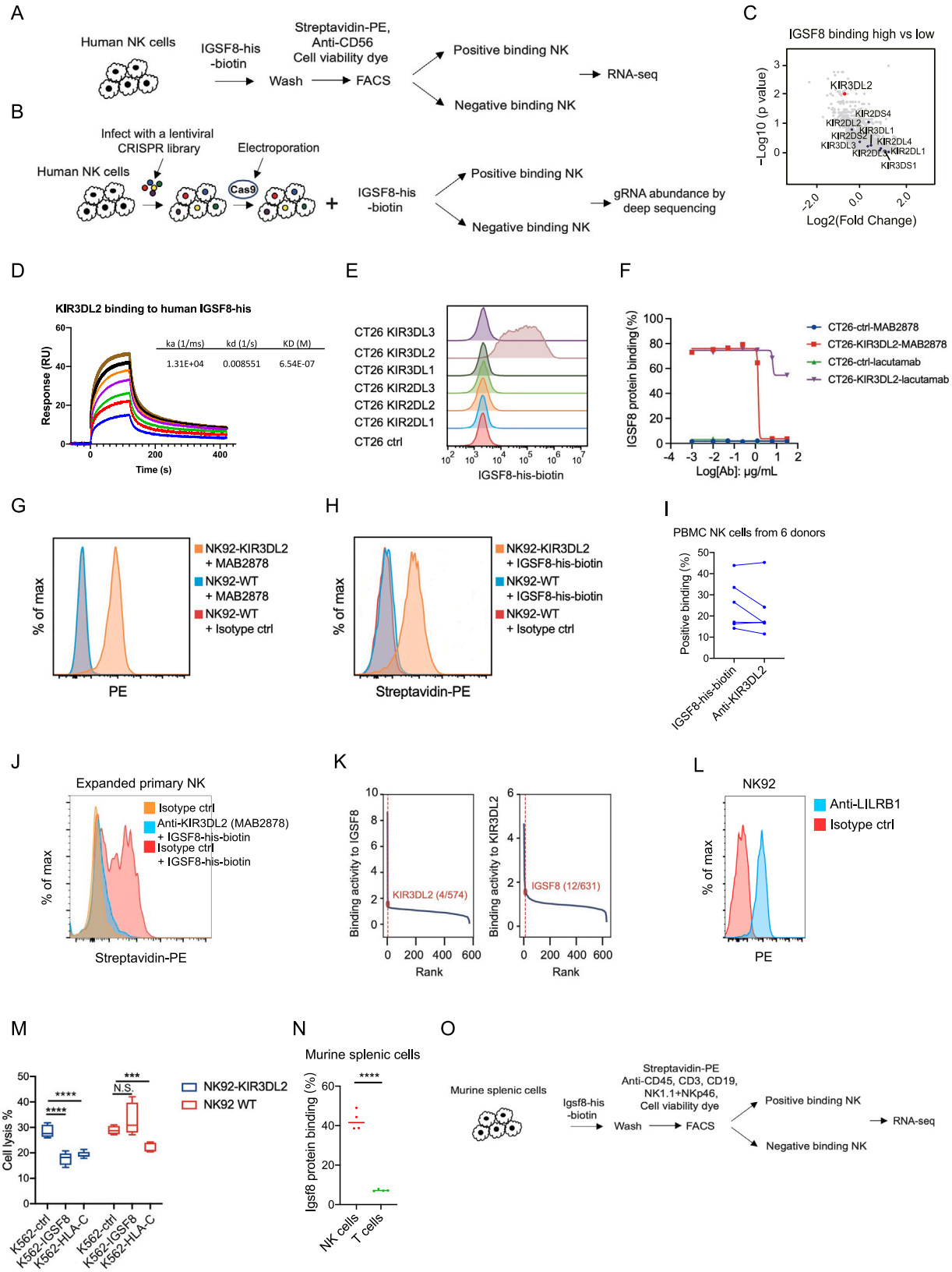

(legend on next page)

Figure S2. Identification of the IGSF8 receptor on human and mouse NK cells, related to Figure 2

(A) Schematic representation of the strategy for using flow cytometry-based RNA-seq to identify the receptor of IGSF8 on human NK cells.

(B) Schematic representation of the strategy for using flow cytometry-based CRISPR screens to identify the receptor of IGSF8 on NK cells.

(C) Negatively selected genes in NK cells with high IGSF8 binding (top 10 percentile) compared to low IGSF8 binding (bottom 10 percentile). The KIR family genes are highlighted.

(D) Surface plasmon resonance (SPR) sensorgrams of the interaction between KIR3DL2 and IGSF8.

(E) Flow cytometry staining of CT26 cells with exogenous expression of six KIR family genes or the HA tag (control) by a lentiviral vector. Overlay histograms show the binding of the IGSF8 proteins to CT26 cells with different KIR family genes or to control cells.

(F) The effect of anti-KIR3DL2 mAbs (MAB2878 from R&D) and Lacutamab on the binding of biotinylated IGSF8-his recombinant protein to CT26 cells transduced with human KIR3DL2 or HA tag (control).

(G and H) Flow cytometry staining with anti-KIR3DL2 monoclonal antibody (G) and biotinylated IGSF8-his protein (H) to stain wild-type NK92 cells or KIR3DL2$^+$ NK92 cells. The KIR3DL2$^+$ NK92 cells were genetically modified to overexpress the KIR3DL2 gene.

(I) Flow cytometry staining was performed on primary PBMC-derived NK cells obtained from 6 healthy donors. In the experiment, CFSE-labeled K562 cells were co-cultured with primary PBMC-derived NK cells at an E:T ratio of 1:1. After 4 h, the cells were stained with anti-CD56, a viability dye, anti-KIR3DL2 antibody (MAB2878), or biotinylated IGSF8 protein. The percentage of IGSF8 protein or MAB2878 binding to live NK cells (CFSE$^-$ CD56$^+$) is presented.

(J) Flow cytometry staining of human NK cells was conducted by simultaneously adding either anti-KIR3DL2 monoclonal antibody (10 μg/mL) or an isotype-matched control Ig (10 μg/mL) with biotinylated IGSF8-his protein (50 μg/mL).

(K) A recent high-throughput interaction screening study[38] of human cell surface receptors identified IGSF8 and KIR3DL2 as each other's mutual top interaction partners. The rank of IGSF8 and KIR3DL2 were highlighted.

(L) Flow cytometry staining of NK92 wild-type cells with anti-LILRB1 mAb and isotype-matched control IgG.

(M) NK92-mediated cytotoxicity against K562 cells with over-expression of IGSF8, HLA-C or HA-tag control by lentiviral delivery. NK cells were either wild-type (red) or engineered to overexpress KIR3DL2 (blue). The data are represented as mean ± SD (n = 5; two-tailed Student's t test).

(N) Flow cytometry analysis was performed on mouse splenic cells using anti-CD45, CD19, CD3, NK1.1 mAbs, a viability dye, and biotinylated mouse Igsf8-his protein. The percentage of Igsf8 binding partner+ cells in splenic T cells (CD45$^+$CD19$^-$NK1.1$^-$CD3$^+$) and splenic NK cells (CD45$^+$CD19$^-$CD3$^-$NK1.1$^+$) is shown (Each dot represents a sample from a mouse, n = 4; two-tailed Student's t test, ***p < 0.001).

(O) A schematic representation of the strategy for using Flow cytometry-based RNA-seq to identify the receptor of Igsf8 on mouse splenic NK cells.

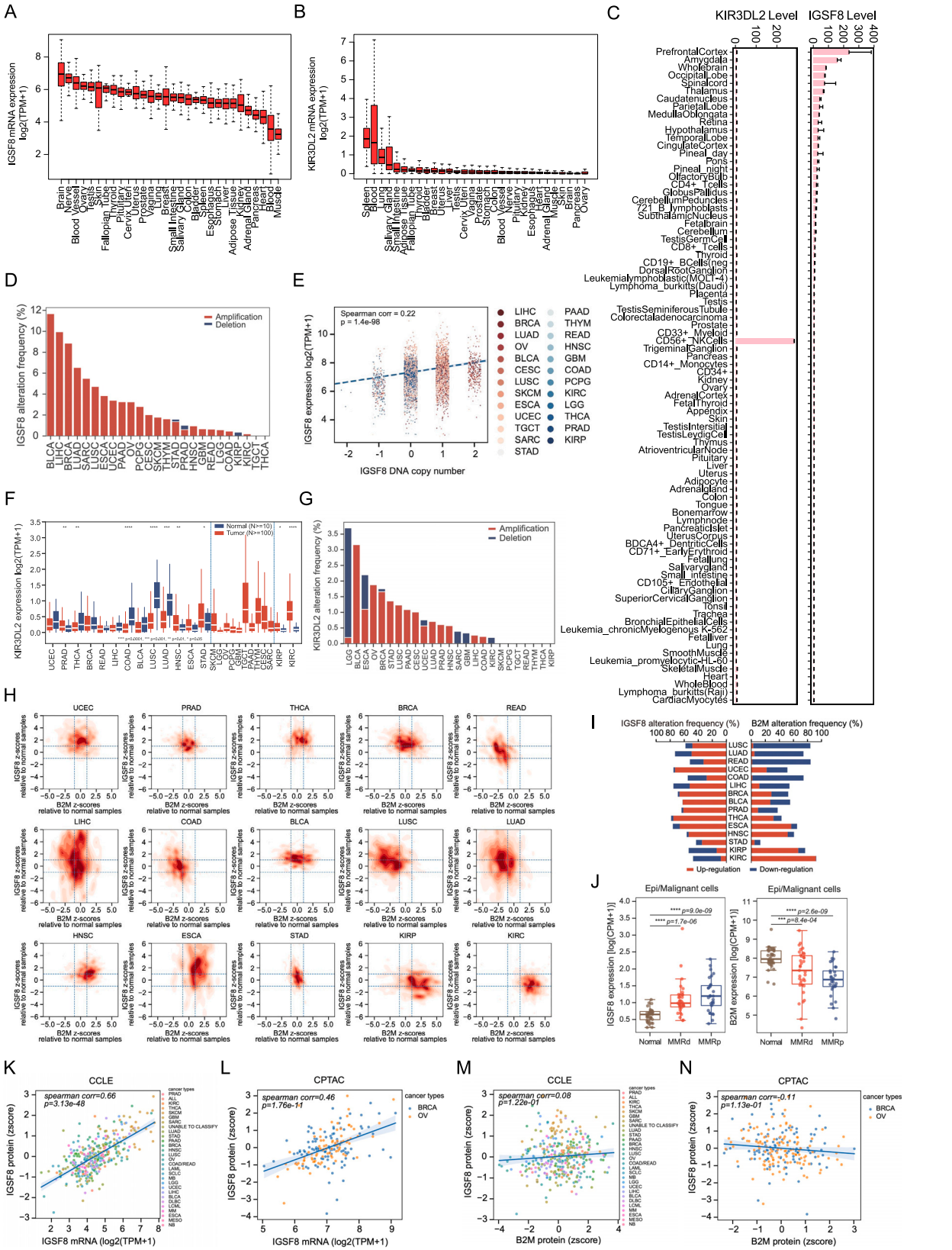

(legend on next page)

Figure S3. Evaluation of IGSF8 and KIR3DL2 gene expression profiles in patient tumors, related to Figure 3

(A) IGSF8 expression level in normal tissues in GTEx data. IGSF8 is most highly expressed in the brain.

(B) Same as (A) for KIR3DL2. KIR3DL2 is most highly expressed in the spleen.

(C) IGSF8 (right) and KIR3DL2 (left) expression patterns in a panel of 79 human tissues. IGSF8 shows the highest expression in the prefrontal cortex and KIR3DL2 is uniquely expressed in $CD56^{+}$ NK cells.

(D) IGSF8 DNA copy number variation in multiple tumor types. Amplification and deletion frequencies are depicted by red and blue bars, respectively. Tumor types are sorted along the X axis by the total copy number alteration frequencies.

(E) The positive correlation between IGSF8 DNA copy number and IGSF8 expression level among all TCGA tumor samples.

(F) Solid tumors (>100 samples, red) and normal tissues (>10 samples, blue) were categorized into three groups (vertical dashed lines) based on differential expression of KIR3DL2 in tumor versus tumor-adjacent normal tissues in TCGA. Tumor-normal pairs are sorted by the tumor expression of KIR3DL2 within each category. Differences assessed by two-tailed Student's t-test: $^{*}p < 0.05$, $^{**}p < 0.01$, $^{****}p < 0.0001$.

(G) KIR3DL2 DNA copy number variation in multiple tumor types. Amplification and deletion frequencies are depicted by red and blue bars, respectively. Tumor types are sorted along the X axis by the total copy number alteration frequency.

(H) Contour plots depicting the distribution of patient samples based on the normalized mRNA expression levels of IGSF8 and B2M across diverse tumor types. The expression values in tumors are normalized to the adjacent normal tissues at the populational level. Dashed lines at z scores −1.0 and 1.0 serve as reference lines on the contour plots.

(I) mRNA alteration frequencies of IGSF8 and B2M in tumors relative to normal tissues (STAR Methods). Alteration frequency is plotted on the x axis, with tumor types sorted on the y axis by the cumulative occurrence of IGSF8 upregulation and B2M downregulation.

(J) Re-analysis of scRNA-seq data of CRC samples in Pelka et al.[47] Boxplots depict the differential expression of IGSF8 and B2M on epithelial/malignant cells at the pseudo bulk level, comparing tumor-adjacent normal tissue, MMRd and MMRp tumors.

(K and L) Scatterplots illustrate the Spearman correlations between IGSF8 protein and mRNA levels, both *in vitro* (K) and in patient tumors (L).

(M and N) Scatterplots demonstrating the Spearman correlations between IGSF8 protein and B2M protein levels, both *in vitro* (M) and in patient tumors (N).

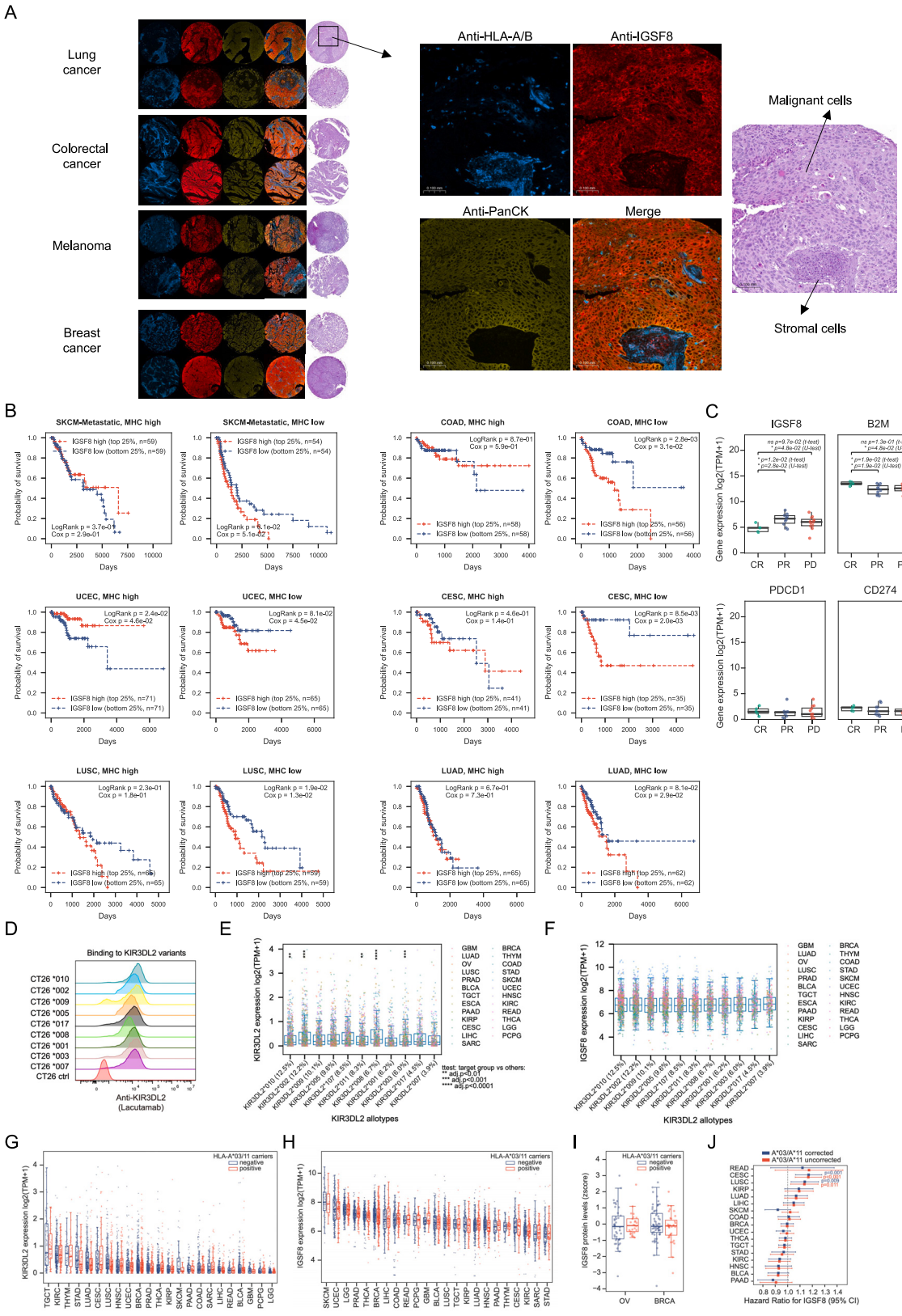

(legend on next page)

Figure S4. The impact of KIR3DL2 or HLA allele variants on the expression profiles of IGSF8 and KIR3DL2 genes in patient tumors, related to Figure 3

(A) Representative images of immunohistochemical staining using anti-IGSF8 (red), anti-HLA-A/B (blue, the antibody may cross-react with HLA-C and HLA-E based on manufacturer's instructions), anti-pan cytokeratin (yellow) antibodies, and H&E, on eight formalin-fixed paraffin-embedded tissue sections of different tumor types (two examples for each tumor type). The "merge" image combines the three antibody colors to demonstrate the co-localization of IGSF8, HLA-A/B, and cytokeratin in the tumor sections. Scale bars, 100 μm.

(B) Kaplan–Meier plots of overall survival in six types of cancer patients with either high antigen presentation (MHC-I high, top 50%) or low antigen presentation (MHC-I low, bottom 50%). Within each group, patients were further divided into IGSF8 high (top 25%), and IGSF8 low (bottom 25%) groups based on their IGSF8 expression levels. The log rank test assessed the difference in overall survival between the IGSF8 high and IGSF8 low populations. Additionally, Cox multivariate regression was performed to evaluate the impact of IGSF8 expression on overall survival, while accounting for patient age, gender, and tumor stage.

(C) Analysis of pretreatment gene expression differences among patients categorized by responses to anti-PD1 treatment. RNA-seq data from the Gene Expression Omnibus (GEO) under accession number GSE78220 [56] was analyzed. CR: complete response, PR: partial response, PD: progressive disease. Statistical analysis used the two-tailed Student's t-test and Wilcoxon rank-sum test to determine the significance of differences.

(D) Flow cytometry staining of CT26 cells with exogenous expression of nine KIR3DL2 variants or the HA tag (control) by a lentiviral vector. Overlay histograms show the binding of Lacutamab to CT26 cells with different KIR3DL2 variants or to control cells.

(E and F) mRNA expression of KIR3DL2 (E) and IGSF8 (F) among patients with different *KIR3DL2* alleles. Differences assessed between patients with or without a specific allele by two-tailed Student's t-test. Multiple hypothesis tests were performed: **adj.$p < 0.01$, ***adj.$p < 0.001$, ****adj.$p < 0.0001$.

(G–I) Expression levels of KIR3DL2 mRNA (G), IGSF8 mRNA (H) and IGSF8 protein (I) between patients with or without HLA-A*03/A*11. No significant differences were observed assessed by two-tailed Student's t-test.

(J) Association between IGSF8 expression and patients' survival with or without considering HLA-A*03 and A*11 as confounding factors. P-values are only shown when IGSF8 hazard ratio is significantly different from one. In the case of CESC and LUSC, the significant differences in hazard ratio from one do not seem to arise from HLA-A*03 and A*11 alleles.

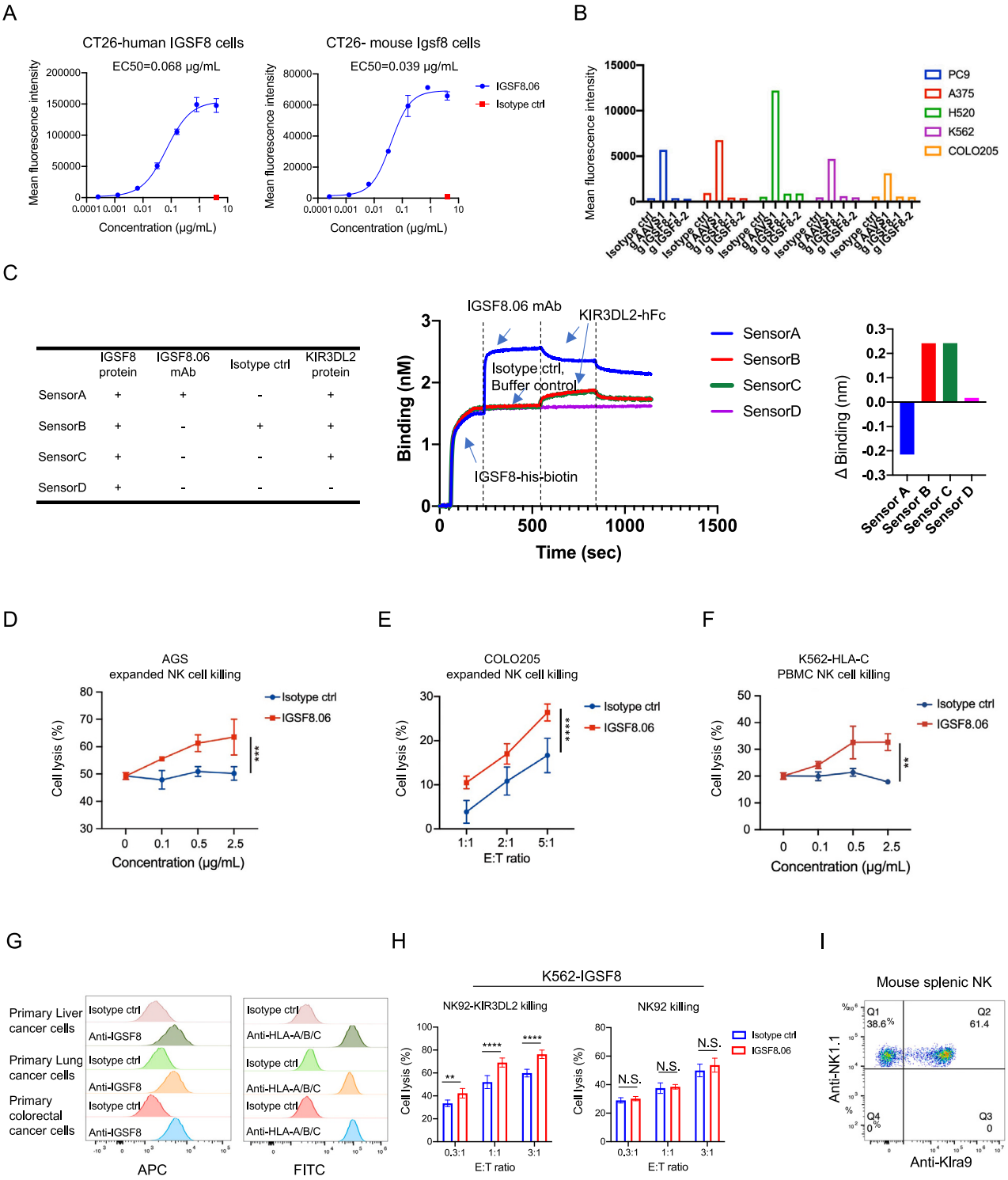

Figure S5. *In vitro* functional assays for an anti-IGSF8 therapeutic antibody, related to Figure 4

(A) Assessment of the IGSF8.06 antibody binding to CT26 cells overexpressing human or mouse IGSF8. Mean fluorescence intensity (MFI) was measured by flow cytometry.

(B) Assessment of the IGSF8.06 antibody binding to PC9, A375, H520, K562, and COLO205 cells with or without endogenous expression of IGSF8. Control (gAAVS1) and perturbation (gIGSF8-1&2) groups are shown on the X axis.

(legend continued on next page)

(C) Biotinylated IGSF8-his protein (50 μg/mL) was immobilized onto streptavidin-coated biosensor tips. Following equilibration, IGSF8.06 mAb (100 μg/mL, SensorA, blue), human IgG1 isotype-matched control (100 μg/mL, SensorB, orange), and buffer control (SensorC, green) were sequentially introduced to the biosensor tips. The binding of IGSF8.06 mAb to SensorA resulted in a significant increase in signal, whereas no binding was observed on the biosensors treated with either the control antibody (SensorB) or buffer alone (SensorC). Subsequently, KIR3DL2-hFc protein (500 μg/mL) was added to the biosensor, resulting in a significant increase (Δ Binding) in signal on the control biosensors (SensorB and SensorC), indicating that KIR3DL2-hFc protein can bind to IGSF8 protein. However, the signal on SensorA, which was previously bound with IGSF8.06 mAb, decreased instead (Δ Binding). The baseline signal (magenta, SensorD) was recorded as buffer control.

(D) Dose-response curve using varying concentrations (x axis) of IGSF8.06-IgG1-LALA (red) or IgG1-LALA isotype-matched control IgG (blue) treatment versus cell lysis (y axis). K562- mbIL21-expanded human NK cells were evaluated against AGS cells at a 1:1 E:T ratio overnight. Results are presented as mean ± SD (n = 3, a two-way ANOVA test, $^{***}p < 0.001$).

(E) Human NK cell-mediated cytotoxicity against COLO205 cells evaluated at the indicated E:T ratios for overnight, in presence of 1 μg/mL of IGSF8.06-IgG1-LALA antibodies and isotype-matched controls. Cytotoxicity results are presented as mean ± SD (n = 6, a two-way ANOVA test, $^{****}p < 0.0001$).

(F) Dose-response curve on the effect of varying concentrations (x axis) of IGSF8.06 (red) or isotype-matched control IgG (blue) (both with IgG1-LALA Fc) treatment on K562-HLA-C cell lysis (y axis). Human primary PBMC NK cells from a healthy donor were co-cultured with K562 cells overexpressing HLA-C at a 1:1 E:T ratio with antibody treatment for 4 h. Results are presented as mean ± SD (n = 3, two-way ANOVA test, $^{**}p < 0.01$).

(G) Flow cytometry staining of primary liver, lung, and colorectal malignant cells with either anti-IGSF8, anti-HLA-A/B/C, or an isotype-matched control antibody to evaluate IGSF8 and MHC-I protein expression.

(H) Engineered NK92-KIR3DL2 cells were co-cultured with K562-IGSF8 overexpressing cells at varying E:T ratios with 1 μg/mL of IGSF8.06-IgG1-LALA or IgG1-LALA isotype control antibody for 4 h. Cytotoxicity results are presented as mean ± SD (n = 5, two-tailed Student's t test, $^{**}p < 0.01$, $^{****}p < 0.0001$).

(I) Flow cytometry staining of mouse splenic NK cells with anti-NK1.1 and anti-Klra9 mAbs.

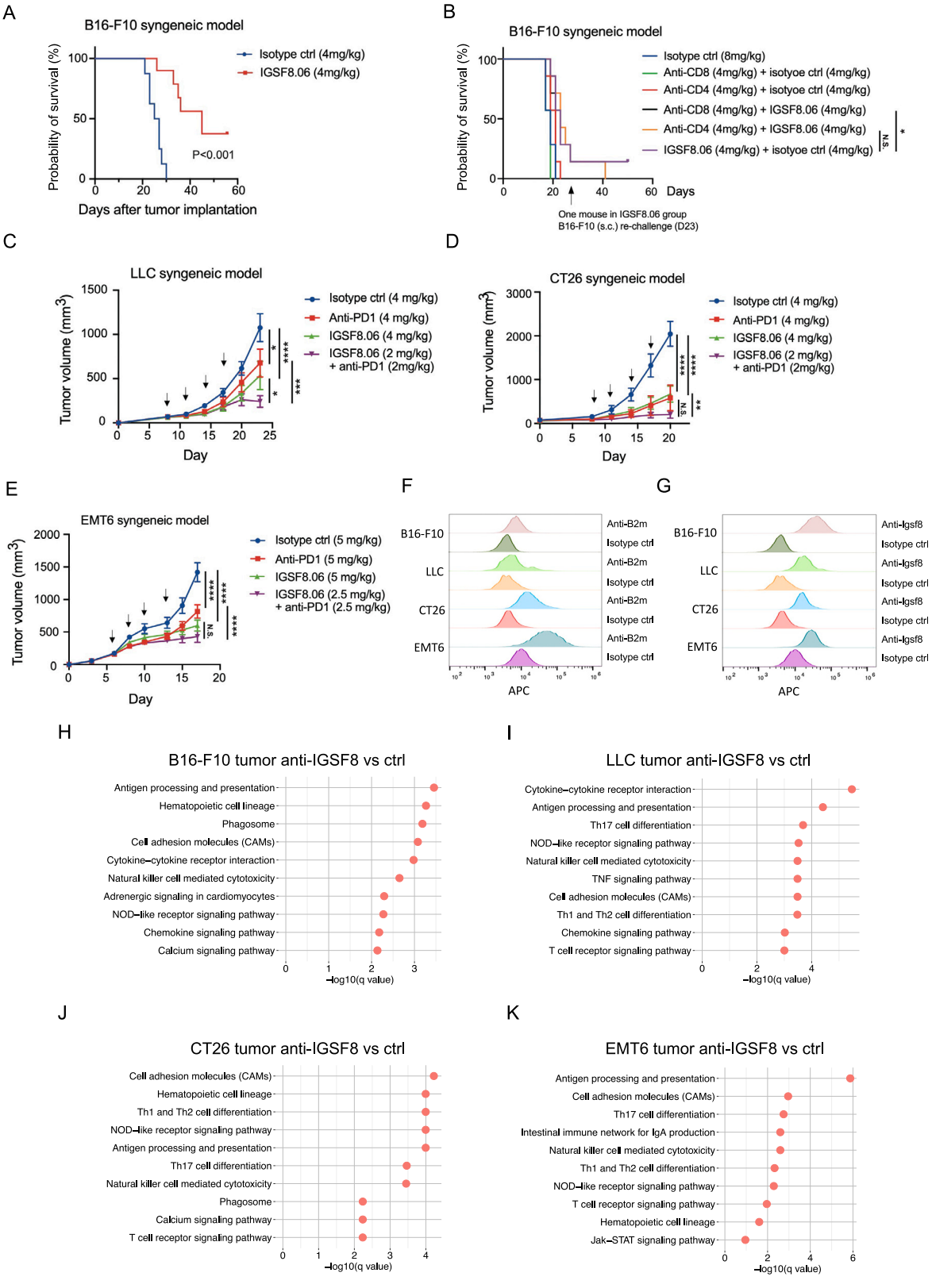

(legend on next page)

Figure S6. The anti-IGSF8 therapeutic antibody inhibits tumor growth by activating NK cells, related to Figure 5

(A) Survival of B16-F10 syngeneic mice in monotherapy treatment with control antibody (blue) and IGSF8.06 (red) (n = 8). Log rank (Mantel-Cox) test was used to determine statistical significance.

(B) Survival of B16-F10 syngeneic mice by anti-CD4 and CD8 depletion in the B16-F10 syngeneic model treated with either IGSF8.06 or isotype-matched antibody controls (n = 7). On day 21, one mouse in the IGSF8.06 monotherapy group showed complete tumor regression. On day 23 (indicated by an arrow), the mouse was re-implanted subcutaneously with 1 million B6-F10 cells. Subsequently, it was observed that the tumor did not reappear in this mouse on day 50. Log rank (Mantel-Cox) test was used to determine statistical significance. *$p < 0.05$.

(C–E) LLC (C), CT26 (D), and EMT6 (E) syngeneic model treated with anti-PD1, IGSF8.06, combination, and isotype-matched controls. The data are presented as mean ± SD (n = 8), and a two-way ANOVA test and Greenhouse-Geisser correction. Dosing was indicated byarrows. **$p < 0.01$, ***$p < 0.005$, ****$p < 0.001$.

(F and G) Flow cytometric staining of B16-F10, LLC, CT26 and EMT6 cells with either anti-mouse Igsf8, anti-B2m, or an isotype-matched control antibody to evaluate their *in vitro* B2m (F) and Igsf8 (G) protein expression.

(H–K), Top enriched KEGG gene pathways of up-regulated genes in B16-F10 (H), LLC (I), CT26 (J), and EMT6 (K) tumors with IGSF8.06 treatment vs. control treatment.